Highly efficient synthetic CRISPR RNA/Cas9-based mutagenesis for cardiovascular phenotypic screening in F0 zebrafish

Rachael E. Quick[1, 2], Sweta Parab[1, 2], Zane R. Tolbert[1, 2] & Ryota L. Matsuoka[1, 2, *]

Affiliations:

[1] Department of Cardiovascular and Metabolic Sciences, Lerner Research Institute, Cleveland Clinic, Cleveland, OH 44195, USA

[2] Department of Molecular Medicine, Cleveland Clinic Lerner College of Medicine, Case Western Reserve University, Cleveland, OH 44195, USA

*Correspondence: Ryota L. Matsuoka (matsuor@ccf.org)

Keywords:

CRISPR/Cas9; genome editing; biallelic mutagenesis; zebrafish; vascular development; blood vessels; perivascular cells

ABSTRACT

The zebrafish is a valuable vertebrate model to study cardiovascular formation and function due to the facile visualization and rapid development of the circulatory system in its externally growing embryos. Despite having distinct advantages, zebrafish have paralogs of many important genes, making reverse genetics approaches inefficient since generating animals bearing multiple gene mutations requires substantial efforts. Here, we present a simple and robust synthetic CRISPR RNA/Cas9-based mutagenesis approach for generating biallelic F0 zebrafish knockouts. Using a dual-guide synthetic CRISPR RNA/Cas9 ribonucleoprotein (dgRNP) system, we show that simultaneous injections of three distinct dgRNPs per gene into one-cell stage embryos dramatically enhanced the efficiency of biallelic gene disruptions with greater consistency than any single dgRNP injections tested on 4 different genes. Importantly, this mutagenesis method is capable of disrupting genes encoding distinct types of proteins, including secreted and membrane-bound forms, and the generated F0 animals fully phenocopied the endothelial and peri-vascular defects observed in corresponding stable mutant homozygotes. Moreover, we provide evidence that this approach faithfully recapitulated the trunk vessel phenotypes resulting from the genetic interaction between two *vegfr2* zebrafish paralogs. Therefore, our approach offers a highly efficient genetic platform to quickly assess novel and redundant gene function in F0 zebrafish.

INTRODUCTION

Over the past few decades, the zebrafish model has provided a powerful screening and live imaging platform to study the mechanisms of cardiovascular development, physiology, and regeneration in vertebrates due to their high fecundity, optical clarity, and regenerative capacity [1-12]. These cardiovascular studies include investigations into 1) transcriptional specification of cardiac and vascular cell types; 2) early phases of cardiac morphogenesis and angioblast migration during vasculogenesis; 3) cardiac differentiation, trabeculation, maturation and regeneration; 4) vascular lumen formation, anastomosis, remodeling and repair; 5) organ-specific angiogenesis and lymphangiogenesis; 6) peri-vascular mural cell origins and migration to vessel walls during development and tissue repair; and 7) mechanical and hemodynamic regulation of these processes. Findings and insights from studies that utilize zebrafish have made substantial contributions to advance our understanding of the vertebrate cardiovascular system in health and disease.

The advent of genome editing tools such as zinc-finger nucleases (ZFNs), transcription activator-like effector nucleases (TALENs), and CRISPR/Cas9 makes it dramatically more convenient to generate targeted zebrafish mutants [13-19], accelerating zebrafish genetic studies using reverse genetics approaches. However, accumulating evidence has suggested that, due to the presence of duplicated genes or adapting genes whose responses are triggered by transcriptional adaptation, knocking out a single gene is not always sufficient to identify gene function through a phenotypic analysis of zebrafish mutants [20-23]. Given the fact that generating zebrafish that carry multiple mutated genes requires time-consuming and labor-intensive genetic crosses and subsequent genotyping, there is an increasing demand and necessity for a reliable and efficient method to quickly test the gene of interest and potential genetic redundancy in F0 animals.

Many studies have reported efficient methods for generating F0 zebrafish mutants using *in vitro*-transcribed guide RNA (gRNA) [24-30], or more recently, using a dual-guide CRISPR/Cas9 ribonucleoprotein (dgRNP) system that utilizes a chemically synthesized duplex of CRISPR RNA (crRNA) and trans-activating crRNA (tracrRNA) [31-37]. However, there is currently no integrated, standardized approach that is well established in the community, making it difficult to select which method to utilize based on the pre-existing and emerging information in the rapidly evolving field. Current evidence suggests that synthetic crRNAs perfectly matched to target sequences achieve much more efficient target cleavage than that which *in vitro*-transcribed gRNAs carrying mismatched nucleotides are able to achieve in zebrafish [31]. This finding reported by Hoshijima *et al*. in late 2019 has allowed the broader use of a synthetic crRNA-based dgRNP method as a potentially more efficient genome editing approach. However, despite the higher efficacy of synthetic crRNAs at cleaving target

sequences in general, their ability to induce monoallelic or biallelic gene inactivation in F0 animals depends on the target sequences of individual designed crRNAs since variable efficiency of crRNAs in gene editing has been reported [37]. Establishing a simple method that ensures maximal efficiency of generating biallelic F0 knockouts without requiring strict crRNA selections will make it user-friendly.

Here we have addressed this issue by integrating some key observations from these prior studies. We specifically focused on assessing the ability of individual and combined synthetic crRNA injections in inducing biallelic knockout phenotypes by targeting multiple genetic loci critical for vascular development, phenotypic readouts that have not been extensively tested using the dgRNP system. We demonstrate that the approach of co-injecting three different dgRNP complexes per gene is capable of disrupting genes encoding distinct types of proteins required for the formation of different vascular cell types with greater efficiency and consistency than any single dgRNP injections examined.

RESULTS

Cytoplasmic injections of three dgRNPs per gene increase the efficiency of generating biallelic F0 knockouts in zebrafish

Like in mammals, blood and lymphatic vessel development in zebrafish relies heavily on the coordinated actions of vascular endothelial growth factor (Vegf) signalling through its cognate Vegf receptors. In the zebrafish genome, two *vegfr2* paralogs exist – *kdrl* and *kdr* [38], making a Vegf receptor family consisting of Flt1, Kdrl, Kdr, and Flt4. Several mutations in *kdrl* have been characterized in regards to their developmental vascular phenotypes, with *kdrl*^{um19} mutants exhibiting a stalling in the sprouting of arterial intersegmental vessels (aISVs) from the dorsal aorta. *kdrl*^{um19} mutants harbor a 4 base pair deletion in exon 2, resulting in a truncated extracellular domain without the receptor tyrosine kinase and transmembrane domains, which is expected to be a null mutant [39].

By analyzing progeny derived from *kdrl*^{um19} heterozygous adult incrosses (Figure 1A), we observed that *kdrl*^{um19} homozygous embryos displayed stalled aISV growth (Figure 1D, 1H), with some reaching the dorsal side of the trunk at 32 hours post fertilization (hpf) as previously reported [39]. In contrast, *kdrl*^{um19} heterozygotes exhibited ISV lengths equivalent to those seen in their WT siblings (Figures 1B, 1C, and 1H). This stalled aISV phenotype observed in *kdrl*^{um19} homozygotes persists at later developmental stages, up to at least 55 hpf (Figures 1E–G). Thus, we chose to utilize this robust and highly penetrant phenotype as a readout to test our approach in assessing monoallelic or biallelic disruption of this gene.

We first tested the efficacy of each designed *kdrl* crRNA by injecting them individually into the cytoplasm of one-cell stage embryos and then carrying out high-resolution melt analysis (HRMA) at 24 hpf (Figures 1I–M). We designed three different crRNAs (Figure 1I), all of which targeted the exons of

kdrl that encode part of the 1st and 2nd immunoglobulin-like domains in the extracellular domain (Figure 1J). We expected that these designed crRNAs would induce mutations that truncate Kdrl in the extracellular domain, resulting in a truncated protein with no receptor function. We validated that these three crRNAs are all capable of disrupting the corresponding target genomic sequences as revealed by HRMA (Figures 1K–M). We injected the three effective crRNAs individually, in the form of dgRNP complexes, into an endothelial-cell specific *Tg(kdrl:EGFP)*^{s843} reporter line to analyze and compare the effect of individual dgRNP complexes on aISV growth at 32 hpf (Figure 1N) – the same developmental stage at which we analyzed embryos from *kdrl*^{um19} heterozygous incrosses. For phenotypic quantifications throughout this study, we chose to analyze only the embryos/larvae that did not display obvious gross morphological defects regardless of being injected or uninjected. We noted that the ISV lengths in these injected embryos varied considerably between the injection groups and also within each injection group. For example, the ISV lengths of fish injected with the *kdrl* crRNA3-containing dgRNP complex closely matched those of the uninjected and Cas9-injected control groups (Figure 1U), indicating that this particular dgRNP complex was not capable of generating biallelic *kdrl* disruptions. In contrast, injections of the dgRNP complex composed of crRNA1 or crRNA2 led to a broader range of aISV lengths (Figure 1U), including the stalled aISV phenotype observed in *kdrl*$^{-/-}$ embryos. However, despite the stalled aISV phenotype, overall average aISV lengths were not comparable to those in *kdrl*$^{-/-}$ embryos, suggesting that injections of individual dgRNP complexes were not efficient at generating biallelic *kdrl* knockouts.

Previous studies showed that increasing the number of injected *in vitro*-transcribed guide RNAs per gene enhanced the efficiency of gene disruption [24]. Based on these data, we next asked whether a simultaneous cytoplasmic injection of the three dgRNP complexes increases the efficiency of *kdrl* gene disruptions. At the one-cell stage, we injected a mixture containing all three dgRNP complexes, each present at the same concentration of crRNAs used for their individual injections. We maintained the constant, equal concentration of Cas9 protein across the individual, combined, and control injection cocktails to make quantitative comparisons. We found that a simultaneous cytoplasmic injection of the three dgRNP complexes dramatically increased the number of embryos exhibiting the stalled aISV phenotype, as examined at 32 and 55 hpf (Figures 1Q–U) without showing apparent gross morphological defects (Figures 1O, 1P). When quantified for aISV lengths, we noted that the average aISV lengths in the embryos injected with the three dgRNP complexes closely resembled those observed in *kdrl*$^{-/-}$ embryos (Figure 1U). These results demonstrate that a cytoplasmic injection of three dgRNPs per gene dramatically enhanced the efficiency of generating biallelic F0 *kdrl* knockouts that recapitulate the early embryonic trunk vascular defect seen in its stable mutant homozygotes.

Cytoplasmic injections of triple *flt4* or *ccbe1* dgRNPs led to a complete loss of a meningeal perivascular cell type as observed in corresponding stable homozygous mutants.

Next, we compared this single and triple dgRNP injection approach by examining a developmental process that occurs at later embryonic/larval stages and that involves another vascular cell type. Fluorescent granular perithelial cells (FGPs) – also called Mato cells [40], meningeal mural lymphatic endothelial cells [41], or brain lymphatic endothelial cells [42] – are a perivascular cell type that resides within the brain meninges. This cell type has been suggested to regulate meningeal angiogenesis and also to guide vascular regeneration after cerebrovascular injury in zebrafish [41, 43]. We hereafter refer to this cell type as FGPs. Zebrafish FGPs were previously shown to emerge from the optic choroidal vascular plexus at 2.5 dpf and migrate along the bilateral mesencephalic veins over the optic tectum by 4 dpf [40-42]. FGPs in zebrafish exhibit molecular signatures similar to those of lymphatic endothelial cells (LECs) and, like LECs, the formation of this cell type depends on the Vegfc/Vegfd/Flt4 signaling axis [41, 42]. Adult *flt4*^{hu4602} mutants were shown to display greatly reduced FGPs, and larvae injected with a morpholino targeting *flt4* exhibited completely absent FGPs at 5 dpf [41].

Since the *flt4*^{hu4602} point mutation in the kinase domain is thought to be hypomorphic, we used fish harboring a 2 base pair deletion in exon 4, the *flt4*^{um131} mutation, which truncates Flt4 in the extracellular domain, thus resulting in a null mutant [20, 44]. To examine FGP formation in *flt4*^{um131} mutants, we incrossed *flt4*^{um131} heterozygous adults and quantified the number of FGPs that form the bilateral loops over the optic tectum in *flt4*$^{+/+}$, *flt4*$^{+/-}$, and *flt4*$^{-/-}$ larvae at 6 dpf (Figures 2A–E) – 2 days after FGP migration over the optic tectum is complete in WT. To quantify the number of FGPs, we employed *Tg(fli1:nEGFP);Tg(lyve1:DsRed)* double transgenic lines that label all endothelial cell nuclei in EGFP and mark lymphatic cell lineages, including FGPs, in DsRed. We counted the number of *Tg(fli1:nEGFP);Tg(lyve1:DsRed)* double-positive cells that comprised the bilateral loops over the optic tectum within the defined areas (Figure S1). We noted that despite the broader range in number of FGPs observed in *flt4*$^{+/-}$ larvae than those in *flt4*$^{+/+}$ fish, the fish of these two genotypes did not show a significant difference in their cell numbers at 6 dpf (Figures 2B, 2C, and 2E). However, all the *flt4*$^{-/-}$ larvae we examined at 6 dpf completely lacked FGPs (Figures 2D and 2E). We used this clear FGP phenotype as another readout to assess the efficiency of single and triple dgRNP injections in generating biallelic disruption of the *flt4* gene.

Similarly to how we validated the *kdrl* crRNAs, we examined the efficacy of each *flt4* crRNA by injecting them individually into one-cell stage embryos and then performing HRMA at 24 hpf (Figures 2F–J). We designed three different crRNAs (Figure 2F), all of which were targeted to the exons of *flt4* that encode part of the 1st and 2nd immunoglobulin-like domains in the extracellular domain (Figure

2G). We thus expected that these designed crRNAs would cause mutations that truncate Flt4 in the extracellular domain, resulting in a truncated protein with no receptor function. These three crRNAs were able to disrupt the corresponding target genomic sequences as revealed by HRMA (Figures 2H–J). We injected each of the three effective crRNAs in the form of dgRNPs individually, or as a mixture, into *Tg(fli1:nEGFP);Tg(lyve1:DsRed)* double transgenic lines to compare the effect of the individual injections versus the triple dgRNP injections on FGP numbers over the optic tectum at 6 dpf (Figure 2K) – the same developmental stage at which we analyzed larvae from *flt4*^{um131} heterozygous incrosses. Under these experimental conditions, single dgRNP injections exhibited varied efficacy. Injections of the dgRNP complex consisting of either crRNA2 or crRNA3 showed broader ranges in FGP numbers than those observed in the uninjected and Cas9-injected control fish at 6 dpf (Figure 2R). Injections of the crRNA1-containing dgRNP complex alone led to an overall reduction of FGP numbers compared to the control groups (Figure 2R). Approximately 32%, 21%, and 71% of larvae injected with the individual dgRNP cocktail consisting of crRNA1, crRNA2, or crRNA3, respectively, failed to form FGPs at 6 dpf. In contrast, combined injections of the three dgRNPs led to a complete absence of FGPs without displaying gross morphological deficits except slight pericardial edema (Figures 2L, 2M) in all injected larvae we examined at 6 dpf (Figures 2N, 2O, and 2R) as observed in *flt4*$^{-/-}$ larvae. This phenotype persisted at later developmental time points, up to at least 10 dpf (Figures 2P, 2Q). These results demonstrate that simultaneous cytoplasmic injections of the triple dgRNP cocktail allowed for highly efficient generation of biallelic F0 *flt4* knockouts, resulting in a complete loss of perivascular FGPs over the optic tectum.

Using exactly the same readout, we next targeted a separate gene encoding the secreted protein Ccbe1. Since the *flt4* gene encodes the membrane-bound receptor Flt4, this experiment combined with the *flt4* dgRNP injection results allowed us to test the utility of a triple dgRNP injection approach in disrupting genes that encode distinct forms of proteins. As previously reported [42], *ccbe1* homozygous, but not heterozygous, mutants displayed a complete loss of FGPs over the optic tectum at 6 dpf (Figures 3A–E and S2). We then injected the three validated crRNAs targeting *ccbe1* (Figures 3F–J) in the form of dgRNPs individually, or simultaneously, into the cytoplasm of one-cell stage *Tg(fli1:nEGFP);Tg(lyve1:DsRed)* embryos (Figure 3K). The phenotypic results were very similar to what we observed in larvae injected with single or the triple *flt4* dgRNPs. Injections of individual *ccbe1* dgRNPs led to more variable FGP phenotypes regardless of the crRNAs. Approximately 68%, 37%, and 90% of larvae injected with the individual dgRNP cocktail consisting of crRNA1, crRNA2, or crRNA3, respectively, failed to form FGPs at 6 dpf. This result is in contrast to the consistent, fully penetrant "No FGP" phenotype in larvae injected with the three combined dgRNPs (Figures 3L–R).

These findings demonstrate that the approach of injecting three dgRNPs per gene is capable of inactivating genes encoding membrane-bound and secreted forms of proteins.

Cytoplasmic injections of triple *vegfab* dgRNPs led to a complete absence of endothelial cells that comprise vertebral arteries as observed in *vegfab* stable homozygous mutants.

A previous study showed that Vegfab is required for the formation of vertebral arteries (VTAs), which develop bilaterally in the ventrolateral locations adjacent to the spinal cord [45]. It was also shown that endothelial cells (ECs) that form the VTAs begin sprouting from the ISVs between 3 and 4 dpf, and that VTA formation is mostly complete by around 7–8 dpf [45]. As reported in this prior study, we observed that VTAs were completely absent in all *vegfab*$^{-/-}$ larvae we examined at 8 dpf (Figure 4A, 4D, and 4E). The same stage of *vegfab*$^{+/-}$ larvae exhibited an overall reduction in number of ECs that comprise VTAs as compared to those observed in *vegfab*$^{+/+}$ fish (Figure 4B, 4C, and 4E). Despite this lower EC number, a vast majority of *vegfab*$^{+/-}$ larvae (near 94%) displayed present VTAs in contrast to the complete absence of VTAs in *vegfab*$^{-/-}$ fish. To quantify the exact number of ECs comprising VTAs, we employed *Tg(kdrl:EGFP);Tg(kdrl:NLS-mCherry)* double transgenic reporters in which blood ECs and their nuclei are marked in EGFP and mCherry, respectively. We used this clean phenotype as another readout to further test the approach of injecting single and triple dgRNPs targeted to the secreted angiogenic ligand Vegfab.

We designed three *vegfab* crRNAs by targeting exons that encode the N-terminal domain or the VEGF homology domain critical for Vegf dimerization and function. These three crRNAs were all designed to target sequences upstream of the mutations harbored in the *vegfab*^{bns92} allele (Figures 4F and 4G). We validated the efficacy of individual *vegfab* crRNAs by injecting each into one-cell stage embryos and then performing HRMA at 24 hpf (Figures 4F–J). We then injected each of the three crRNAs individually, or simultaneously, into the cytoplasm of one-cell stage *Tg(kdrl:EGFP);Tg(kdrl:NLS-mCherry)* embryos to compare the effect of individual and the combined three dgRNP injections on VTA formation at 8 dpf (Figure 4K). We injected Cas9 protein without a duplex of crRNAs and tracrRNAs as a control. We noted that each of the three dgRNPs targeting *vegfab* was highly efficient at abrogating VTA formation, however, there were still some larvae in each injection group that formed VTAs. Approximately 50%, 85%, and 40% of larvae injected with the individual dgRNP cocktail consisting of crRNA1, crRNA2, or crRNA3, respectively, failed to form VTAs at 8 dpf. In contrast, all larvae injected with the three dgRNP cocktail exhibited a complete absence of VTAs at 8 dpf (Figures 4M, 4O and 4R) unlike Cas9 alone-injected control fish at the same stage that exhibited mostly formed VTAs (Figure 4L, 4N and 4R). This absent VTA phenotype persisted at later developmental stages, up to at least 12 dpf (Figures 4P and 4Q). These results provide

another example of highly-efficient gene disruption via simultaneous cytoplasmic injection of three dgRNPs targeting the secreted protein, leading to a defect in blood EC development in the trunk.

Yolk injections of three dgRNPs per gene allowed efficient generation of biallelic F0 knockouts. The dgRNP injection results we showed thus far were all performed via cytoplasmic injections at the one-cell stage. This selection of injection sites is based on an original study that injected a RNP complex composed of synthetic crRNA, tracrRNA, and Cas9 protein into the cytoplasm for mutagenesis in zebrafish [31]. A recent study showed that injection of synthetic dgRNP complexes into the yolk of one-cell stage embryos is also highly effective [32]. However, the importance of injection sites has yet to be experimentally addressed by injecting the same set of dgRNP complexes. Thus, we next investigated this issue by utilizing exactly the same preparations of dgRNP complexes and also the same phenotypic readouts that were used for the cytoplasmic injection experiments in order to compare these data to yolk injection experiments.

First, we tested yolk injections of the three dgRNPs targeting *flt4* or *ccbe1* by examining the number of FGPs that comprised the bilateral loops over the optic tectum at 6 dpf (Figure 5A). We noted that *flt4* and *ccbe1* triple dgRNP injections into the yolk were both highly efficient at abrogating FGP formation. All *Tg(fli1:*nEGFP*);Tg(lyve1:*DsRed*)* larvae injected with the three dgRNPs targeting *flt4* via the yolk completely lacked the FGPs at 6 dpf (Figures 5B and 5C). This result is exactly the same as the fully penetrant "No FGP" phenotype achieved by their cytoplasmic injections. On the other hand, we observed that 4 out of 28 larvae (approximately 14%) injected with the three dgRNPs targeting *ccbe1* via the yolk formed FGPs similar to Cas9 alone-injected sibling controls, while the remaining larvae displayed a complete loss of FGPs over the optic tectum. Given the fact that none of the larvae injected with the same three dgRNPs targeting *ccbe1* via the cytoplasm formed FGPs, cytoplasmic injections may lead to more consistent and efficient results than yolk injections.

Second, we investigated yolk injections of the three dgRNPs targeting *vegfab* by examining the number of ECs that comprised VTAs at 8 dpf (Figure 5D). We noted that 25 out of 27 larvae (approximately 93%) injected with the three dgRNPs displayed a complete lack of VTAs. However, the remaining 2 fish showed sprouting vessels at the locations where VTAs normally develop (Figures 5E and 5F). These sprouting vessels were not observed in the larvae injected with the same three dgRNPs targeting *vegfab* via the cytoplasm, indicating that cytoplasmic injections may have a higher efficiency and consistency. Taken together, these results demonstrate that yolk injections of three dgRNPs per gene enabled efficient generation of biallelic F0 knockouts, although their cytoplasmic injections may perform with even greater efficiency and reproducibility (a summary table shown in Figure 5G).

Genetic interaction analysis of functionally redundant genes using triple dgRNP injections. An increasing amount of evidence has shown that duplicated or related genes in zebrafish play redundant roles in regulating certain biological processes. This high level of redundancy among multiple functionally-related proteins may not allow one to observe overt phenotypes when only single genes are genetically eliminated. This lack of a phenotype in single gene knockouts often requires us to generate double and triple genetic mutants to find phenotypes, making phenotypic analyses of genetic mutants more laborious. Examining transcriptionally-adapting genes in the absence of a certain functional gene would be helpful to narrow down potential candidates that compensate for the loss of gene function. However, it is important to establish an efficient functional assay to quickly test these candidate genes for the sake of ones' time, commitment, and resources.

We therefore asked whether our highly-efficient mutagenesis approach for generating biallelic F0 knockouts can provide a platform for rapid screening of potential genetic interactions. To test this idea, we examined the genetic interactions between two Vegfr2 zebrafish paralogs, Kdrl and Kdr, in trunk vascular development. Previous studies using morpholinos targeting *kdrl* and *kdr* suggest that co-injections of these two morpholinos led to a much more severe defect in aISV formation than their individual injections [38, 46]. In addition, a separate study showed that injecting a *kdr* morpholino into *kdrl* mutants led to a similar, severe aISV formation defect [47]. These studies suggest that Kdrl and Kdr are functionally redundant in regulating aISV formation.

To examine this genetic interaction, we measured aISV lengths in $kdr^{+/+}$, $kdr^{+/-}$, and $kdr^{-/-}$ embryos and also the same genotypes of embryos in the $kdrl^{-/-}$ genetic background at 32 hpf (Figure 6A). We noted that while deleting one or two copies of *kdr* in WT background did not lead to any apparent defect in aISV development (Figures 6B–D, 6H, and 6I), doing the same in the $kdrl^{-/-}$ genetic background dramatically exacerbated this phenotype (Figures 6E–G, 6H, and 6I). In $kdr^{+/+};kdrl^{-/-}$ embryos, stalled aISV growth was noted (Figure 6E), consistent with the earlier observations (Figures 1B–D and 1H). The same stage of $kdr^{+/-};kdrl^{-/-}$ embryos exhibited more prominent aISV formation defects, leading to much shorter aISV lengths and a partial absence of the dorsal aorta in approximately 9% of fish (Figures 6F, 6H, and 6I). Trunk vessel defects were even more severe in $kdr^{-/-};kdrl^{-/-}$ embryos, resulting in a complete absence of the dorsal aorta in all the 32 hpf embryos we examined (Figures 6G, 6H, and 6I). This enhanced expressivity of aISV and dorsal aorta phenotypes by deleting one or two copies of *kdr* in the $kdrl^{-/-}$ genetic background demonstrates the strong genetic interaction between *kdr* and *kdrl*.

Next, we tested this genetic interaction by injecting Cas9 protein alone or the three dgRNPs targeting *kdrl* into the cytoplasm of one-cell stage embryos derived from $kdr^{+/-}$ incrosses (Figure 6J).

This approach allowed us to compare aISV lengths in injected embryos of *kdr*$^{+/+}$, *kdr*$^{+/-}$, or *kdr*$^{-/-}$ genotypes without generating double mutant animals. We noted that Cas9-injected control embryos did not display any overt trunk vessel defects regardless of the *kdr* genotypes (Figures 6K–M, 6Q, and 6R), consistent with the earlier observations (Figures 6B–D, 6H, and 6I). In contrast, simultaneous cytoplasmic injections of the three dgRNPs resulted in varying degrees of trunk vessel defects. Subsequent genotyping and quantification results showed that, similar to what we observed in *kdr*$^{+/-}$*;kdrl*$^{-/-}$ embryos, *kdr*$^{+/-}$ embryos injected with the three dgRNPs exhibited significantly shorter average lengths of aISVs than those of the dgRNPs-injected *kdr*$^{+/+}$ siblings (Figures 6N, 6O, and 6R). In addition, approximately 16% of the dgRNPs-injected *kdr*$^{+/-}$ embryos displayed a partial absence of the dorsal aorta (Figure 6Q). In the dgRNPs-injected *kdr*$^{-/-}$ embryos, we noted that nearly 48% and 19% of them showed a complete absence and a partial absence of the dorsal aorta, respectively (Figures 6P and 6R). Given the fact that an absent dorsal aorta phenotype was observed only in *kdr*$^{-/-}$*;kdrl*$^{-/-}$, or the dgRNPs-injected *kdr*$^{-/-}$, embryos, this mutagenesis approach allowed efficient biallelic disruption of *kdrl* with his experimental setup as well. Collectively, we provided quantitative evidence that our mutagenesis approach faithfully recapitulated the genetic interaction results observed in embryos carrying mutations in both *kdr* and *kdrl*, offering a functional screening platform to test potential genetic redundancy.

DISCUSSION

Here we present a simple and robust genetic approach that enables the generation of biallelic F0 zebrafish knockouts in a highly efficient fashion. We provided evidence that this approach is capable of inactivating genes that encode different forms of proteins critical for endothelial and peri-vascular cell development occurring in distinct parts of the body during the period spanning from early embryonic to later larval stages. This method is user-friendly and affordable since minimal efforts on testing a mutagenic activity of designed crRNAs would be required before starting F0 functional screens of the genes of interest, and these crRNAs can be also used to generate stable genetic mutants, including indel and deletion mutants. We were indeed able to successfully generate *ccbe1* stable mutants shown in this study by utilizing one of its designed crRNAs (Figure S2). Synthetic crRNAs are highly effective since we designed a total number of 14 different synthetic crRNAs in this study, 13 of which disrupted the corresponding target genomic region revealed by HRMA. Morpholinos have been utilized to silence gene function in F0 embryos [48, 49], however they cannot be employed to generate genetic mutants. Moreover, the presented method is capable of inactivating gene function over much longer time periods than relatively shorter, limited time windows of morpholinos' gene silencing activity, allowing for wider

applications in F0 screens, ranging from early developmental to later physiological and complex behavioral processes. We discuss the advantages of our approach compared to previously reported methods and also describe a few potential applications of this approach.

Injections of single vs triple dgRNPs per gene

While dgRNP-based mutagenesis utilizing chemically synthesized crRNAs have been shown to efficiently disrupt gene function in F0 zebrafish even as single dgRNP injections [31-37], it is becoming clear that the efficacy of target gene disruption depends on the mutagenic ability of each designed crRNA, as also suggested by the recent report showing variable efficiency of synthetic crRNAs in gene editing [37]. As such, injection of single dgRNPs per gene can lead to varied mutagenesis efficiency, resulting in variable and incosistent phenotypic observations across crRNAs targeted to the same gene in injected F0 animals. This was indeed what we experienced. Taking a single crRNA injection approach may thus require significant efforts for selection and validation of crRNAs before starting F0 screens.

In this study, we have addressed this issue and established a simple method that maximizes the efficiency of creating biallelic F0 knockouts with a requirement of minimal efforts on checking a mutagenic activity of designed crRNAs by HRMA or alternative method(s). To establish this method, we integrated some critical findings from the earlier studies, including those made by Hoshijima et al. [31] and Wu et al. [24]. To achieve rigorous phenotypic quantifications in each injected or uninjected animal, we selected three distinct phenotypic readouts involved in vascular development that are easily quantifiable. Phenotypic comparisons by these quantifiable readouts: 1) provided precise information on phenotypic variations between individual animals; 2) allowed us to evaluate the ability and efficiency of individual and combined dgRNP injections in inducing knockout phenotypes; and 3) determined the most efficient mutagenesis approach to recapitulate homozygous stable mutant phenotypes.

We found that individual dgRNP injections mostly led to variable phenotypes with only some exhibiting high potency (Figure 5G), suggesting that careful assessments of a selected crRNA's activity would be needed if a single dgRNP was injected. This finding is consistent with a recent study noting variable mutagenic efficiency of crRNAs [37]. We also compared the site of injections (cytoplasm vs yolk) since a recently published work using a similar approach performed injections exclusively into the yolk to examine behavioral phenotypes [32]. Our results showed that although three dgRNP injections into either site were both highly efficient, their cytoplasmic injections were slightly more consistent in phenocopying homozygous stable mutant phenotypes. Together, our data provided quantitative evidence that cytoplasmic co-injections of three dgRNPs per gene achieve biallelic gene disruptions with the highest efficiency and consistency in F0 zebrafish among all of the tested conditions.

Quick phenotypic screening and validation of the genes of interest

Zebrafish females have remarkably high fecundity and can produce a large number of offspring per spawning session. Combined with rapid external development and optical transparency of zebrafish embryos, these features have made zebrafish an ideal vertebrate model for large-scale, high-throughput genetic and chemical screenings to identify new genes and pathways fundamental to vertebrate development [50, 51]. The optimized method we describe here can be used as an alternative, or supplemental, approach to these genetic and chemical screening methods. For example, our described method can be used as a secondary genetic assay for validation of key compounds that are identified via phenotype-based small molecule screening using zebrafish embryos. This approach can be also used to quickly test potential candidate genes that have been narrowed down after conducting forward genetic screens and subsequent genetic mapping of causative loci. This fast, robust, and affordable approach can be utilized for a broad range of experimental assays as a primary, secondary, or tertiary method to screen and/or validate the gene of interest, facilitating functional genomic analyses in zebrafish.

Rapid functional screening of genetically interacting genes or transcriptionally adapting genes

The large number of duplicated genes in the zebrafish genome has made it more laborious to perform a phenotypic screening of zebrafish mutants generated via a reverse genetics approach. Moreover, recent evidence suggests that the deleterious mutations introduced into the zebrafish genome via genome editing can trigger genetic compensatory machinery through transcriptional adaptation, a process by which transcriptional modulation of related genes, termed adapting genes, is induced [21-23]. Due to these complex genetic interaction networks in zebrafish, there is an increasing demand for a rapid screening platform to dissect the roles of duplicated or adapting genes with redundant or compensatory functions. As a proof of concept, we have provided evidence that our triple dgRNP injection approach addressed the functional redundancy in regulating trunk axial vessel and aISV formation between two duplicated *vegfr2* zebrafish genes, *kdrl* and *kdr*, in a manner comparable to that is observed in their double mutants. Thus, this approach enables fast functional screening of genetically interacting genes or adapting genes prior to generating zebrafish that harbor multiple mutated genes.

Validation of new research tools

We expect that our presented approach can also be utilized to quickly validate new research tools created in labs, including custom-made antibodies and dominant-negative forms of proteins. For example, the specificity of custom-made antibodies can be tested in biallelic F0 knockouts generated via this method. Genes encoding the protein of interest can be disrupted by this method, if their mutants are not available immediately. In this way, a researcher can forgo at least 3-6 months of testing the

specificity of antibodies in mutants that may be imported from elsewhere or generated from scratch. Global or tissue/cell-specific overexpression of dominant-negative forms of proteins has been commonly used to abrogate signaling in zebrafish [52-56]. The efficacy of dominant-negative forms of proteins can be rapidly assessed by comparing results to phenotypes observed in biallelic F0 knockouts generated via this method, even without immediately available mutants. Hence, this approach will be useful to quickly test an array of new research tools that may need knockout zebrafish samples to address specificity and reliablity.

Altogether, our highly-efficient mutagenesis approach for creating biallelic F0 zebrafish knockouts will provide a valuable platform to conduct a rapid analysis and validation of gene function and redundancy, as well as of research tools, in labs utilizing zebrafish and possibly other genetic animal models.

Acknowledgements

We thank Drs. Didier Stainier and Nathan Lawson for kindly providing us with fish lines; Don Zeisloft and his team for zebrafish care and husbandry; Drs. Judith Drazba, John Peterson, Gauravi Deshpande, and Ajay Zalavadia for imaging. This work was supported by funding from the National Institutes of Health (R01 NS117510) and start-up funds from the Cleveland Clinic Foundation to R.L.M.

Author Contributions

R.E.Q. and R.L.M. designed and performed experiments, analyzed data, and wrote the manuscript; S.P. and Z.T. performed experiments and analyzed data. All authors commented on the manuscript.

Conflict of Interest

The authors declare that they have no conflict of interest.

Data Availability

All relevant data will be fully available without restriction and provided within the manuscript and its supporting information files.

Materials and methods

Zebrafish husbandry and strains. All zebrafish husbandry was performed under standard conditions in accordance with institutional and national ethical and animal welfare guidelines. All zebrafish work was approved by the Cleveland Clinic's Institutional Animal Care and Use Committee under the protocol number 2018-1970. The following lines were used in this study: *Tg(kdrl:EGFP)*^{s843} [57]; *Tg(lyve1:DsRed)*^{nz101} [58]; *Tg(fli1:nEGFP)*^{y7} [59]; *Tg(kdrl:NLS-mCherry)*^{is4} [60]; *kdrl*^{um19} [39]; *flt4*^{um131} [20]; *vegfab*^{bns92} [61]; and *kdr*^{bns32} [62]. Adult fish were maintained on a standard 14 h light/10 h dark daily cycle. Fish embryos/larvae were raised at 28.5°C. To prevent skin pigmentation, 0.003% phenylthiourea (PTU) was used beginning at 10-12 hpf for imaging. *flt4* or *ccbe1* dgRNP-injected larvae analyzed at 10 dpf were transferred to a tank containing approximately 250 mL system water supplemented with 0.003% PTU (up to 25 larvae/tank) and fed with Larval AP100 (<50 microns dry diet, Zeigler) starting at 5 dpf. *vegfab* dgRNP-injected larvae analyzed at 8 and 12 dpf were transferred to a tank containing approximately 250 mL system water without PTU (up to 25 larvae/tank) and fed with Larval AP100 (<50 microns dry diet, Zeigler) starting at 5 dpf.

Genotyping of mutants. Genotyping of *kdrl*^{um19},*flt4*^{um131}, *vegfab*^{bns92}, and *kdr*^{bns32} mutant fish was performed by high-resolution melt analysis of PCR products using the following primers:
kdrl um19 forward: 5' – TGCTTCCTGATGGAGATACACACC – 3'
kdrl um19 reverse 5' – TGCAAATGAGTGTGAGTGTCCCAC – 3'
flt4 um131 forward: 5' – GACCATCTTCATAACAGACTCTG – 3'
flt4 um131 reverse: 5' – GGATCTGAAACCAGACATGGTAC – 3'
vegfab bns92 forward: 5'– GTGCTGGGTGCTGCAATG – 3'
vegfab bns92 reverse: 5'– CCAAGGTAATGTTGTATGTGACG – 3'
kdr bns32 forward: 5' – GACCTCACCCTGAGTCCACA – 3'
kdr bns32 reverse 5' – GCGGTGCAGTTGAGTATGAG – 3'

Generation and genotyping of *ccbe1* mutants. The *ccbe1*^{lri97} mutant allele was generated by targeted genome editing using the CRISPR/Cas9 system as follows: We targeted the first exon of *ccbe1*, which encodes the N-terminal part of the Ccbe1 protein-coding sequences prior to the EGF domain. The *ccbe1*^{lri97} mutant allele harbors a 6 base pair deletion and a 1 base pair insertion. The *ccbe1*^{lri97} allele is predicted to carry a frameshift mutation that alters the reading frame of Ccbe1 at threonine residue 26, leading to a premature stop codon after 40 missense amino acids. The following sequences of *ccbe1* CRISPR RNA (crRNA) were used to generate the mutants:

ccbe1 crRNA: TTCTCCTCTCGGAAAGTCCA

Ribonucleoprotein (RNP) complexes of crRNA, trans-activating RNA (tracrRNA), and Cas9 protein were prepared as previously described [31, 63] and described in detail in the method section of crRNA preparations and injections. Injection cocktails (4 μL) containing the crRNA:tracrRNA:Cas9 RNP complexes were prepared as follows: 0.4 μL 25 μM crRNA:tracrRNA, 0.4 μL 25 μM Cas9 protein stock, 2.8 μL H_2O, and 0.4 μL 0.5% phenol red solution (Sigma). Prior to microinjection, injection cocktails were incubated at 37°C for 5 min and then kept at room temperature. Approximately 1 nL of the injection cocktails was injected into the cytoplasm of one-cell stage embryos. Genotyping of *ccbe1*^{lri97} mutant fish was performed by high-resolution melt analysis of PCR products using the following primers:

ccbe1 lri97 forward: 5' – ACTGTTCTCATCGGGAGCTCCGTG – 3'

ccbe1 lri97 reverse: 5' – agcactttacCTGTCTACATCCTC – 3'

High-resolution melt analysis. Embryos injected with individual crRNA-containing RNP complexes were subjected to genomic DNA extraction at 24 hpf. Primer sequences used to analyze the efficacy of individual crRNAs in their injected embryos are listed in Table 1. Fish embryos/larvae carrying stable genetic mutations were collected and subjected to genomic DNA extraction immediately after confocal imaging. A CFX96 Touch Real-Time PCR Detection System (Bio-Rad) was used for PCR reactions and high-resolution melt analysis. Precision Melt Supermix for high-resolution melt analysis (Bio-Rad) was used in these experiments. PCR reaction protocols were: 95°C for 2 min, 46 cycles of 95°C for 10 s, and 60°C for 30 s. Following the PCR, a high-resolution melt curve was generated by collecting EvaGreen fluorescence data in the 65–95°C range. The analyses were performed on normalized derivative plots.

crRNA preparations and injections.

For *kdrl, flt4*, *ccbe1,* and *vegfab* crRNA injections, crRNA:tracrRNA:Cas9 RNP complexes were prepared as previously described [31, 63]. Briefly, duplex buffer (Integrated DNA Technologies, IDT) was used to make a 100 μM stock solution of individual crRNA and tracrRNA. Each crRNA stock solution (100 μM) was mixed with an equal volume of tracrRNA (100 μM) and annealed in a PCR machine as previously described [31] to generate crRNA:tracrRNA duplex complexes (50 μM). 50 μM crRNA:tracrRNA duplex solution was diluted in duplex buffer to generate 25 μM stock solution, which was stored at -20°C. Target genomic locations and sequences of each designed crRNA are listed in Table 1.

25 μM stock solution of Cas9 protein (S.p. Cas9 nuclease, V3, IDT) was prepared as previously described [31]. Injection cocktails (4 μL) containing three different crRNA:tracrRNA:Cas9 RNP complexes were prepared as follows: 0.4 μL 25 μM crRNA1:tracrRNA, 0.4 μL 25 μM crRNA2:tracrRNA, 0.4 μL 25 μM crRNA3:tracrRNA, 1.2 μL 25 μM Cas9 protein stock, 1.2 μL H_2O, and 0.4 μL 0.5% phenol red solution. Injection cocktails (4 μL) containing individual crRNA:tracrRNA:Cas9 RNP complexes were prepared as follows: 0.4 μL 25 μM crRNA:tracrRNA, 1.2 μL 25 μM Cas9 protein stock, 2 μL H_2O, and 0.4 μL 0.5% phenol red solution. Control injection cocktails (4 μL) without cRNA:tracrRNA duplex complexes were prepared as follows: 1.2 μL 25 μM Cas9 protein stock, 2.4 μL H_2O, and 0.4 μL 0.5% phenol red solution. All injection cocktails were freshly prepared on the day of injection and contained a constant, equal concentration of Cas9 protein to make quantitative comparisons. Prior to microinjection, all injection cocktails were incubated at 37°C for 5 min and then kept at room temperature. Approximately 2 nL of the injection cocktails was injected into the cytoplasm or yolk of one-cell stage embryos. For phenotypic quantifications throughout this study, we chose to analyze only the embryos/larvae that did not display obvious gross morphological defects regardless of being injected or uninjected.

Microscopy imaging. A Leica TCS SP8 confocal laser scanning microscope (Leica) was used for live imaging. Live zebrafish embryos and larvae were anaesthetized with a low dose of tricaine, embedded in a layer of 1% low melt agarose in a glass-bottom Petri dish (MatTek), and imaged using a 25X water immersion objective lens. Leica Application Suite X (LAS X) software (Version 3.7.0.20979) was used for image acquisition and analysis.

Quantification of arterial intersegmental vessel (aISV) lengths. *Tg(kdrl:EGFP)*^{s843} reporter fish were used to quantify the lengths of aISVs. For the quantification of aISVs in *kdrl*$^{+/+}$, *kdrl*$^{+/-}$, and *kdrl*$^{-/-}$ embryos at 32 hpf, *kdrl*^{um19} heterozygous adults carrying the *Tg(kdrl:EGFP)* reporter were incrossed. For the genetic interaction experiments, *kdrl*$^{um19/+}$;*kdr*$^{bns32/+}$ adults carrying the *Tg(kdrl:EGFP)* reporter were incrossed, and the generated progeny were analyzed for aISV lengths at 32 hpf. For the *kdrl* crRNA injection experiments, WT or *kdr*^{bns32} heterozygous adults carrying the *Tg(kdrl:EGFP)* reporter were incrossed, and injection cocktails containing Cas9 protein with and without crRNA(s):tracrRNA duplex complexes were injected into the cytoplasm of one-cell stage progeny generated from these crosses. For each fish, the lengths of 5 aISVs in the left side of the trunk region directly anterior to the anal opening were measured using the scale bar tool in LAS X software. aISV measurements began at

the dorsal surface of the dorsal aorta, ending at either the dorsal tip of the aISV or at the connection of the aISV and dorsal longitudinal anastomotic vessel.

Quantification of perivascular FGPs in the dorsal meningeal compartment over the optic tectum. *Tg(fli1:nEGFP)*^{y7}*;Tg(lyve1:DsRed)*^{nz101} reporter fish were used to quantify the number of FGPs in the dorsal meningeal compartment over the optic tectum at 6 dpf. For the quantification of FGPs in *flt4*$^{+/+}$, *flt4*$^{+/-}$, and *flt4*$^{-/-}$ larvae at 6 dpf, *flt4*^{um131} heterozygous adults carrying the *Tg(fli1:nEGFP);Tg(lyve1:DsRed)* reporters were incrossed. For the quantification of FGPs in *ccbe1*$^{+/+}$, *ccbe1*$^{+/-}$, and *ccbe1*$^{-/-}$ larvae at 6 dpf, *ccbe1*^{lri97} heterozygous adults carrying the *Tg(fli1:nEGFP);Tg(lyve1:DsRed)* reporters were incrossed. For the *flt4* and *ccbe1* crRNA injection experiments, *Tg(fli1:nEGFP);Tg(lyve1:DsRed)* adults were incrossed, and injection cocktails containing Cas9 protein with and without crRNA(s):tracrRNA duplex complexes were injected into the cytoplasm or yolk of one-cell stage progeny generated from these crosses as indicated in related figures and legends. *Tg(fli1:*nEGFP*);Tg(lyve1:*DsRed*)*-double positive FGPs were quantified by counting the number of *Tg(fli1:*nEGFP*)*$^{+}$ nuclei in these double-positive cells. LAS X software was utilized to define the region used for this quantification. In the maximum projection confocal images, 150 μm distances from the midline on both sides of the head were measured to set the defined caudolateral area for quantifications across samples (see Figure S2 for the defined areas used to quantify FGPs in this study). The midline corresponds to the region at which the bilateral mesencephalic veins converge. The most lateral point of this line denoted the cutoff point for countable double-positive cells; cells medial to this line were included in the count. Next, 75 μm distances from the midline on both sides were measured to set the defined rostrolateral area for quantifications. The rostral extension of the *Tg(lyve1:*DsRed*)*$^{+}$ loop intersects this line, and this point serves as the most lateral cutoff point for quantification of double positive cells; cells medial to this line were included in the count. Refer to Figure S2 for further information.

Quantification of the number of the endothelial cells that form vertebral arteries (VTAs). *Tg(kdrl:EGFP)*^{s843}*;Tg(kdrl:NLS-mCherry)*^{is4} reporter fish were used to quantify the number of endothelial cells (ECs) that form VTAs at 8 dpf. For the quantification of EC number in *vegfab*$^{+/+}$, *vegfab*$^{+/-}$, and *vegfab*$^{-/-}$ larvae at 8 dpf, *vegfab*^{bns92} heterozygous adults carrying the *Tg(kdrl:EGFP);Tg(kdrl:NLS-mCherry)* reporters were incrossed. For the *vegfab* crRNA injection experiments, *Tg(kdrl:EGFP);Tg(kdrl:NLS-mCherry)* adults were incrossed, and injection cocktails containing Cas9 protein with and without crRNA(s):tracrRNA duplex complexes were injected into the

cytoplasm or yolk of one-cell stage progeny generated from these crosses as indicated in related figures and legends. *Tg(kdrl:*EGFP*);Tg(kdrl:*NLS-mCherry*)*-double positive ECs that comprise VTAs were quantified by counting the number of *Tg(kdrl:*NLS-mCherry*)*$^{+}$ nuclei in these double-positive ECs. The 5 somites directly anterior to the anal opening were examined on both sides of the body (defined as a 5 somite region) to quantify the number of ECs comprising the VTAs at 8 dpf.

Statistical analysis. Statistical differences for mean values among multiple groups were determined using a one-way analysis of variance (ANOVA) followed by Tukey's multiple comparison test. Statistical differences for mean values between two groups were determined using a two-tailed Student's *t*-test. Fisher's exact test was used to determine significance when comparing the degree of penetrance of observed phenotypes. Statistical analyses were performed using GraphPad Prism 8.1.1. The criterion for statistical significance was set at $P < 0.05$. Error bars are SD.

Table 1. crRNA target sites and HRMA primers used to analyze each crRNA-injected embryos.

crRNA Name	Location	Target Sequence [PAM]	Forward Primer (5' left – 3' right)	Reverse Primer (5' left – 3' right)
kdrl crRNA1	Exon 2	GTGTCCCACCAACATGCTGA[AGG]	TCTCGTCTGCCTGATCCACAACTG	ggatgcagtacCTGCAAATGAGTG
kdrl crRNA2	Exon 3	TGTGGACACTTCATGATCGC[TGG]	CAACGACACTGGCATCTACTCATG	cCTTTAACAAAAACATATGTGGAC
kdrl crRNA3	Exon 5	AAATTCTGCGTTATCCACCC[TGG]	TAAAACCTTATGACAGCTACCATC	GCCTTTTAAGTAGGTAGACTGATG
flt4 crRNA1	Exon 3	GCCTGATTTCTCTATACCCT[GGG]	AGTTTACTGATCGCCAGGGTCAGC	TTTTCCAGCCACCCCTTGACACTC
flt4 crRNA2	Exon 3	AATGCCCAGGCCAATGACTC[GGG]	AACCCTACTGCAAGATCTTAATAC	TCAATAACAGCTTTAATGTCCTTG
flt4 crRNA3	Exon 6	GCACTGGTCGACTTCAACAC[TGG]	AGTTGATGCAGGGGGAGAGTTTGG	CTTTTTGCCTGGATAGTCCCACTG
ccbe1 crRNA1	Exon 1	TTCTCCTCTCGGAAAGTCCA[CGG]	CGTGGCGCTCGTACTGTTCTCATC	agcactttacCTGTCTACATCCTC
ccbe1 crRNA2	Exon 2	TACCCGTGCGTAAAGTCCAC[TGG]	TTCAGAAAGCAAAATCGCAACGAC	cgcgtttacCTGTAGCATGTGGTC
ccbe1 crRNA3	Exon 3	CTTCTGGAATACACTGACCC[AGG]	AAGAAGTGCTGTGAAGGTTTCAAG	gagtaatcttacCTTCTGGAATAC
vegfab crRNA1	Exon 1	GAAGCGTCACAATAAATAAC[TGG]	attcaatcATGAACTTTGCTGTTC	TTGACAGCTGAAAAATACAGAAGC
vegfab crRNA2	Exon 2	AGTGCCTACATACCCAGAGA[GGG]	tttacacagAGTGCCTACATAC	aactcacCGTCATATGTGCTTC
vegfab crRNA3	Exon 3	TTGTTATACACCTCCATGAA[TGG]	tcaattttataattcgcagTAGTG	CTGCTGAATTTCCACCAACATTTC

REFERENCES

1. Gore AV, Monzo K, Cha YR, Pan W, Weinstein BM. Vascular development in the zebrafish. Cold Spring Harb Perspect Med. 2012;2(5):a006684.
2. Matsuoka RL, Stainier DYR. Recent insights into vascular development from studies in zebrafish. Curr Opin Hematol. 2018;25(3):204-11.
3. Bakkers J. Zebrafish as a model to study cardiac development and human cardiac disease. Cardiovasc Res. 2011;91(2):279-88.
4. Cao J, Poss KD. The epicardium as a hub for heart regeneration. Nat Rev Cardiol. 2018;15(10):631-47.
5. Kikuchi K, Poss KD. Cardiac regenerative capacity and mechanisms. Annu Rev Cell Dev Biol. 2012;28:719-41.
6. Herbert SP, Stainier DY. Molecular control of endothelial cell behaviour during blood vessel morphogenesis. Nat Rev Mol Cell Biol. 2011;12(9):551-64.
7. Hogan BM, Schulte-Merker S. How to Plumb a Pisces: Understanding Vascular Development and Disease Using Zebrafish Embryos. Dev Cell. 2017;42(6):567-83.
8. Boselli F, Freund JB, Vermot J. Blood flow mechanics in cardiovascular development. Cell Mol Life Sci. 2015;72(13):2545-59.
9. Donadon M, Santoro MM. The origin and mechanisms of smooth muscle cell development in vertebrates. Development. 2021;148(7).
10. Szymborska A, Gerhardt H. Hold Me, but Not Too Tight-Endothelial Cell-Cell Junctions in Angiogenesis. Cold Spring Harb Perspect Biol. 2018;10(8).
11. Park C, Kim TM, Malik AB. Transcriptional regulation of endothelial cell and vascular development. Circ Res. 2013;112(10):1380-400.
12. Nakajima H, Mochizuki N. Flow pattern-dependent endothelial cell responses through transcriptional regulation. Cell Cycle. 2017;16(20):1893-901.
13. Hwang WY, Fu Y, Reyon D, Maeder ML, Tsai SQ, Sander JD, et al. Efficient genome editing in zebrafish using a CRISPR-Cas system. Nat Biotechnol. 2013;31(3):227-9.
14. Huang P, Xiao A, Zhou M, Zhu Z, Lin S, Zhang B. Heritable gene targeting in zebrafish using customized TALENs. Nat Biotechnol. 2011;29(8):699-700.
15. Sander JD, Cade L, Khayter C, Reyon D, Peterson RT, Joung JK, et al. Targeted gene disruption in somatic zebrafish cells using engineered TALENs. Nat Biotechnol. 2011;29(8):697-8.
16. Cade L, Reyon D, Hwang WY, Tsai SQ, Patel S, Khayter C, et al. Highly efficient generation of heritable zebrafish gene mutations using homo- and heterodimeric TALENs. Nucleic Acids Res. 2012;40(16):8001-10.
17. Meng X, Noyes MB, Zhu LJ, Lawson ND, Wolfe SA. Targeted gene inactivation in zebrafish using engineered zinc-finger nucleases. Nat Biotechnol. 2008;26(6):695-701.
18. Doyon Y, McCammon JM, Miller JC, Faraji F, Ngo C, Katibah GE, et al. Heritable targeted gene disruption in zebrafish using designed zinc-finger nucleases. Nat Biotechnol. 2008;26(6):702-8.
19. Foley JE, Yeh JR, Maeder ML, Reyon D, Sander JD, Peterson RT, et al. Rapid mutation of endogenous zebrafish genes using zinc finger nucleases made by Oligomerized Pool ENgineering (OPEN). PLoS One. 2009;4(2):e4348.
20. Kok FO, Shin M, Ni CW, Gupta A, Grosse AS, van Impel A, et al. Reverse genetic screening reveals poor correlation between morpholino-induced and mutant phenotypes in zebrafish. Dev Cell. 2015;32(1):97-108.
21. El-Brolosy MA, Kontarakis Z, Rossi A, Kuenne C, Gunther S, Fukuda N, et al. Genetic compensation triggered by mutant mRNA degradation. Nature. 2019;568(7751):193-7.
22. Rossi A, Kontarakis Z, Gerri C, Nolte H, Holper S, Kruger M, et al. Genetic compensation induced by deleterious mutations but not gene knockdowns. Nature. 2015;524(7564):230-3.
23. Ma Z, Zhu P, Shi H, Guo L, Zhang Q, Chen Y, et al. PTC-bearing mRNA elicits a genetic compensation

response via Upf3a and COMPASS components. Nature. 2019;568(7751):259-63.
24. Wu RS, Lam, II, Clay H, Duong DN, Deo RC, Coughlin SR. A Rapid Method for Directed Gene Knockout for Screening in G0 Zebrafish. Dev Cell. 2018;46(1):112-25 e4.
25. Shah AN, Davey CF, Whitebirch AC, Miller AC, Moens CB. Rapid reverse genetic screening using CRISPR in zebrafish. Nat Methods. 2015;12(6):535-40.
26. Varshney GK, Pei W, LaFave MC, Idol J, Xu L, Gallardo V, et al. High-throughput gene targeting and phenotyping in zebrafish using CRISPR/Cas9. Genome Res. 2015;25(7):1030-42.
27. Jao LE, Wente SR, Chen W. Efficient multiplex biallelic zebrafish genome editing using a CRISPR nuclease system. Proc Natl Acad Sci U S A. 2013;110(34):13904-9.
28. Tsarouchas TM, Wehner D, Cavone L, Munir T, Keatinge M, Lambertus M, et al. Dynamic control of proinflammatory cytokines Il-1beta and Tnf-alpha by macrophages in zebrafish spinal cord regeneration. Nat Commun. 2018;9(1):4670.
29. Xu B, Tang X, Jin M, Zhang H, Du L, Yu S, et al. Unifying developmental programs for embryonic and postembryonic neurogenesis in the zebrafish retina. Development. 2020;147(12).
30. Burger A, Lindsay H, Felker A, Hess C, Anders C, Chiavacci E, et al. Maximizing mutagenesis with solubilized CRISPR-Cas9 ribonucleoprotein complexes. Development. 2016;143(11):2025-37.
31. Hoshijima K, Jurynec MJ, Klatt Shaw D, Jacobi AM, Behlke MA, Grunwald DJ. Highly Efficient CRISPR-Cas9-Based Methods for Generating Deletion Mutations and F0 Embryos that Lack Gene Function in Zebrafish. Dev Cell. 2019;51(5):645-57 e4.
32. Kroll F, Powell GT, Ghosh M, Gestri G, Antinucci P, Hearn TJ, et al. A simple and effective F0 knockout method for rapid screening of behaviour and other complex phenotypes. Elife. 2021;10.
33. Kotani H, Taimatsu K, Ohga R, Ota S, Kawahara A. Efficient Multiple Genome Modifications Induced by the crRNAs, tracrRNA and Cas9 Protein Complex in Zebrafish. PLoS One. 2015;10(5):e0128319.
34. Davis AE, Castranova D, Weinstein BM. Rapid Generation of Pigment Free, Immobile Zebrafish Embryos and Larvae in Any Genetic Background Using CRISPR-Cas9 dgRNPs. Zebrafish. 2021.
35. Klatt Shaw D, Mokalled MH. Efficient CRISPR/Cas9 mutagenesis for neurobehavioral screening in adult zebrafish. G3 (Bethesda). 2021.
36. Zhao D, Jones JL, Gasperini RJ, Charlesworth JC, Liu GS, Burdon KP. Rapid and efficient cataract gene evaluation in F0 zebrafish using CRISPR-Cas9 ribonucleoprotein complexes. Methods. 2021.
37. Keatinge M, Tsarouchas TM, Munir T, Porter NJ, Larraz J, Gianni D, et al. CRISPR gRNA phenotypic screening in zebrafish reveals pro-regenerative genes in spinal cord injury. PLoS Genet. 2021;17(4):e1009515.
38. Bahary N, Goishi K, Stuckenholz C, Weber G, Leblanc J, Schafer CA, et al. Duplicate VegfA genes and orthologues of the KDR receptor tyrosine kinase family mediate vascular development in the zebrafish. Blood. 2007;110(10):3627-36.
39. Covassin LD, Siekmann AF, Kacergis MC, Laver E, Moore JC, Villefranc JA, et al. A genetic screen for vascular mutants in zebrafish reveals dynamic roles for Vegf/Plcg1 signaling during artery development. Dev Biol. 2009;329(2):212-26.
40. Venero Galanternik M, Castranova D, Gore AV, Blewett NH, Jung HM, Stratman AN, et al. A novel perivascular cell population in the zebrafish brain. Elife. 2017;6.
41. Bower NI, Koltowska K, Pichol-Thievend C, Virshup I, Paterson S, Lagendijk AK, et al. Mural lymphatic endothelial cells regulate meningeal angiogenesis in the zebrafish. Nat Neurosci. 2017;20(6):774-83.
42. van Lessen M, Shibata-Germanos S, van Impel A, Hawkins TA, Rihel J, Schulte-Merker S. Intracellular uptake of macromolecules by brain lymphatic endothelial cells during zebrafish embryonic development. Elife. 2017;6.
43. Chen J, He J, Ni R, Yang Q, Zhang Y, Luo L. Cerebrovascular Injuries Induce Lymphatic Invasion into Brain Parenchyma to Guide Vascular Regeneration in Zebrafish. Dev Cell. 2019;49(5):697-710 e5.
44. Shin M, Male I, Beane TJ, Villefranc JA, Kok FO, Zhu LJ, et al. Vegfc acts through ERK to induce

sprouting and differentiation of trunk lymphatic progenitors. Development. 2016;143(20):3785-95.
45. Matsuoka RL, Rossi A, Stone OA, Stainier DYR. CNS-resident progenitors direct the vascularization of neighboring tissues. Proc Natl Acad Sci U S A. 2017;114(38):10137-42.
46. Bridge G, Monteiro R, Henderson S, Emuss V, Lagos D, Georgopoulou D, et al. The microRNA-30 family targets DLL4 to modulate endothelial cell behavior during angiogenesis. Blood. 2012;120(25):5063-72.
47. Covassin LD, Villefranc JA, Kacergis MC, Weinstein BM, Lawson ND. Distinct genetic interactions between multiple Vegf receptors are required for development of different blood vessel types in zebrafish. Proc Natl Acad Sci U S A. 2006;103(17):6554-9.
48. Nasevicius A, Ekker SC. Effective targeted gene 'knockdown' in zebrafish. Nat Genet. 2000;26(2):216-20.
49. Bedell VM, Westcot SE, Ekker SC. Lessons from morpholino-based screening in zebrafish. Brief Funct Genomics. 2011;10(4):181-8.
50. Lawson ND, Wolfe SA. Forward and reverse genetic approaches for the analysis of vertebrate development in the zebrafish. Dev Cell. 2011;21(1):48-64.
51. Zon LI, Peterson RT. In vivo drug discovery in the zebrafish. Nat Rev Drug Discov. 2005;4(1):35-44.
52. Matsuoka RL, Marass M, Avdesh A, Helker CS, Maischein HM, Grosse AS, et al. Radial glia regulate vascular patterning around the developing spinal cord. Elife. 2016;5.
53. Lewis JL, Bonner J, Modrell M, Ragland JW, Moon RT, Dorsky RI, et al. Reiterated Wnt signaling during zebrafish neural crest development. Development. 2004;131(6):1299-308.
54. Shin D, Shin CH, Tucker J, Ober EA, Rentzsch F, Poss KD, et al. Bmp and Fgf signaling are essential for liver specification in zebrafish. Development. 2007;134(11):2041-50.
55. Hubner K, Cabochette P, Dieguez-Hurtado R, Wiesner C, Wakayama Y, Grassme KS, et al. Wnt/beta-catenin signaling regulates VE-cadherin-mediated anastomosis of brain capillaries by counteracting S1pr1 signaling. Nat Commun. 2018;9(1):4860.
56. Kirchgeorg L, Felker A, van Oostrom M, Chiavacci E, Mosimann C. Cre/lox-controlled spatiotemporal perturbation of FGF signaling in zebrafish. Dev Dyn. 2018;247(10):1146-59.
57. Jin SW, Beis D, Mitchell T, Chen JN, Stainier DY. Cellular and molecular analyses of vascular tube and lumen formation in zebrafish. Development. 2005;132(23):5199-209.
58. Okuda KS, Astin JW, Misa JP, Flores MV, Crosier KE, Crosier PS. lyve1 expression reveals novel lymphatic vessels and new mechanisms for lymphatic vessel development in zebrafish. Development. 2012;139(13):2381-91.
59. Roman BL, Pham VN, Lawson ND, Kulik M, Childs S, Lekven AC, et al. Disruption of acvrl1 increases endothelial cell number in zebrafish cranial vessels. Development. 2002;129(12):3009-19.
60. Wang Y, Kaiser MS, Larson JD, Nasevicius A, Clark KJ, Wadman SA, et al. Moesin1 and Ve-cadherin are required in endothelial cells during in vivo tubulogenesis. Development. 2010;137(18):3119-28.
61. Rossi A, Gauvrit S, Marass M, Pan L, Moens CB, Stainier DY. Regulation of Vegf signaling by natural and synthetic ligands. Blood. 2016.
62. Mullapudi ST, Boezio GLM, Rossi A, Marass M, Matsuoka RL, Matsuda H, et al. Disruption of the pancreatic vasculature in zebrafish affects islet architecture and function. Development. 2019;146(21).
63. Parab S, Quick RE, Matsuoka RL. Endothelial cell type-specific molecular requirements for angiogenesis drive fenestrated vessel development in the brain. Elife. 2021;10.

Figure 1

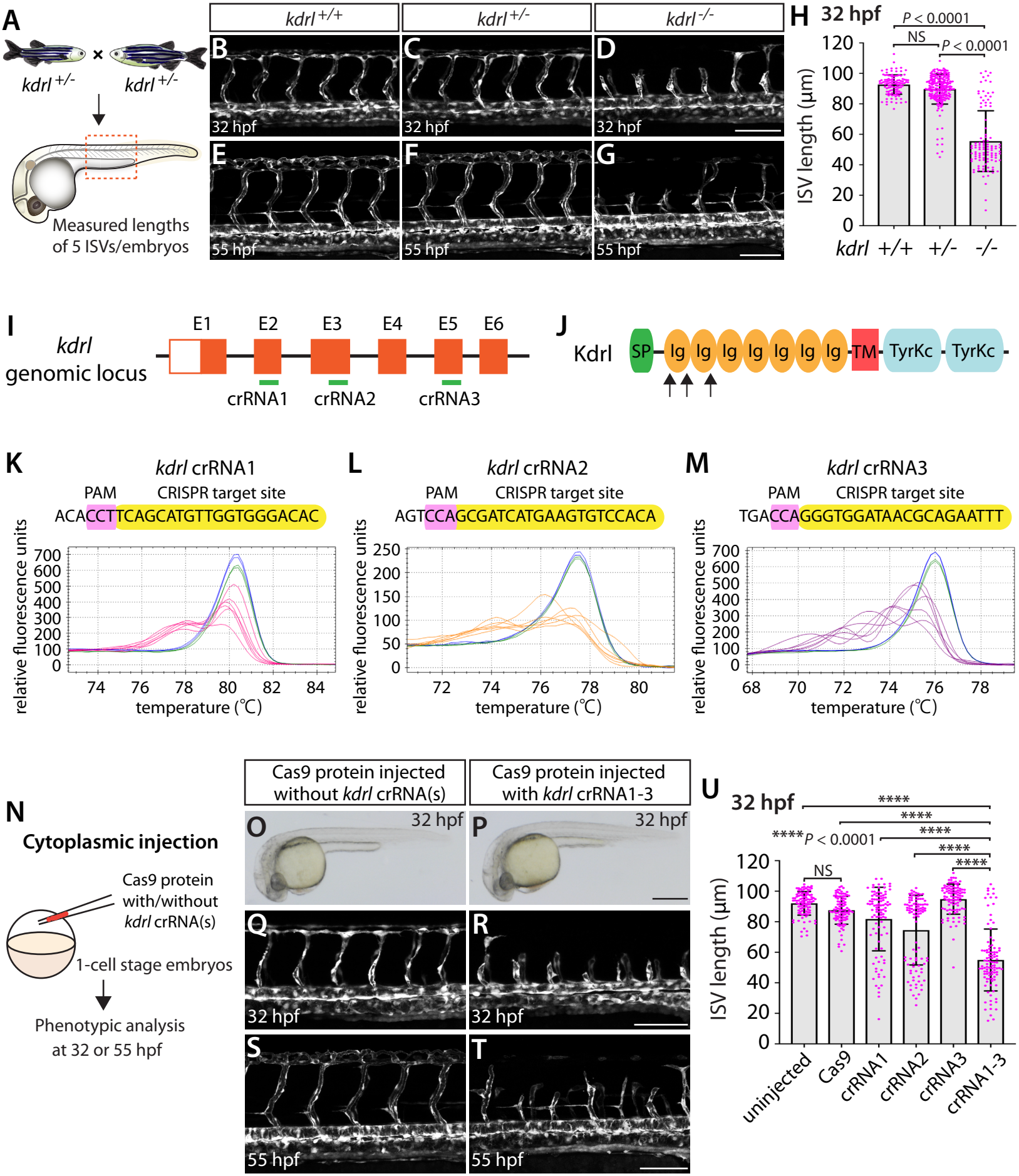
A
kdrl +/-
kdrl +/-
Measured lengths of 5 ISVs/embryos
kdrl +/+
kdrl +/-
kdrl -/-
B
C
D
E
F
G
32 hpf
55 hpf
H
32 hpf
P < 0.0001
NS
P < 0.0001
ISV length (µm)
kdrl +/+ +/- -/-
I
kdrl genomic locus
E1 E2 E3 E4 E5 E6
crRNA1 crRNA2 crRNA3
J
Kdrl
SP Ig Ig Ig Ig Ig Ig Ig TM TyrKc TyrKc
K
kdrl crRNA1
PAM CRISPR target site
ACACCTTCAGCATGTTGGTGGGACAC
relative fluorescence units
temperature (℃)
L
kdrl crRNA2
PAM CRISPR target site
AGTCCAGCGATCATGAAGTGTCCACA
relative fluorescence units
temperature (℃)
M
kdrl crRNA3
PAM CRISPR target site
TGACCAGGGTGGATAACGCAGAATTT
relative fluorescence units
temperature (℃)
N
Cytoplasmic injection
Cas9 protein with/without kdrl crRNA(s)
1-cell stage embryos
Phenotypic analysis at 32 or 55 hpf
Cas9 protein injected without kdrl crRNA(s)
Cas9 protein injected with kdrl crRNA1-3
O
P
Q
R
S
T
32 hpf
55 hpf
U
32 hpf
****
****
****P < 0.0001
****
****
****
NS
ISV length (µm)
uninjected
Cas9
crRNA1
crRNA2
crRNA3
crRNA1-3

Figure 1. Embryos injected with the triple dgRNPs targeting *kdrl* exhibited ISV defects similar to those observed in *kdrl*$^{-/-}$ fish.

(**A**) Experimental setup for the phenotypic analysis presented in panels (**B**–**H**). Adult *kdrl*$^{+/-}$ fish were incrossed, and progeny generated from the crosses were imaged to measure the lengths of arterial intersegmental vessels (aISVs) at 32 hpf.

(**B**–**G**) Lateral views of *kdrl*$^{+/+}$ (**B**, **E**), *kdrl*$^{+/-}$ (**C**, **F**), and *kdrl*$^{-/-}$ (**D**, **G**) trunk vasculature visualized by *Tg(kdrl:*EGFP*)* expression at 32 (**B**–**D**) and 55 (**E**–**G**) hpf.

(**H**) Quantification of aISV lengths in *kdrl*$^{+/+}$, *kdrl*$^{+/-}$, and *kdrl*$^{-/-}$ embryos at 32 hpf (n=23 for *kdrl*$^{+/+}$, n=45 for *kdrl*$^{+/-}$, and n=21 for *kdrl*$^{-/-}$ fish). Lengths of 5 aISVs per embryo were measured. NS: not significant.

(**I**) Three synthetic CRISPR RNAs (crRNAs) were designed to target sequences within exon 2 (E2), E3, and E5 on the *kdrl* genomic locus.

(**J**) Predicted domain structure of zebrafish Kdrl. Kdrl consists of a signal peptide (SP), seven immunoglobulin-like domains (Ig), a transmembrane domain (TM), and two tyrosine kinase domains (TyrKc). Arrows indicate the approximate positions of the protein sequences corresponding to the target sequences of the three designed crRNAs.

(**K**–**M**) High-resolution melt analysis used to validate the efficacy of the three designed crRNAs. The melting curves of 6 independent embryos injected with the dgRNP complex consisting of *kdrl* crRNA1 (**K**, **pink**), crRNA2 (**L**, **orange**), or crRNA3 (**M**, **purple**) are presented. The melting curves of 2 independent, uninjected (**K**–**M**, **blue**) and Cas9 protein-injected (**K**–**M**, **green**) sibling embryos are also presented for comparison for each crRNA. Injection of each dgRNP cocktail disrupted the corresponding target genomic sequences.

(**N**) Experimental workflow of the microinjection experiments for panels (**O**–**S**). Injection cocktails containing Cas9 protein with and without the individual or the three *kdrl* crRNA:tracrRNA duplex complexes were injected into the cytoplasm of one-cell stage *Tg(kdrl:EGFP)* embryos. Injected *Tg(kdrl:EGFP)* progeny were analyzed for ISV formation at 32 and 55 hpf.

(**O** and **P**) Brightfield images of the 32 hpf embryos injected with Cas9 protein with (**P**) or without (**O**) the three *kdrl* crRNA:tracrRNA duplex complexes (crRNA1-3).

(**Q**–**T**) Lateral trunk views of the 32 (**Q**, **R**) and 55 (**S**, **T**) hpf *Tg(kdrl:EGFP)* fish injected with Cas9 protein with (**R**, **T**) or without (**Q**, **S**) the three *kdrl* crRNA1-3. While aISVs in Cas9 protein alone-injected embryos fused at the dorsal side of the trunk to begin forming the dorsal longitudinal anastomotic vessel by 32 hpf (**Q**), a vast majority of aISVs in the embryos injected with the triple *kdrl* dgRNPs failed to reach the dorsal side of the trunk (**R**). This aISV stalling phenotype was observed at later developmental stages, including at 55 hpf (**T**).

(**U**) Quantification of aISV lengths for each injection and uninjection group at 32 hpf (n=20 fish for each control and injection group; 5 aISV lengths per embryo measured). Average aISV lengths of the triple dgRNPs-injected embryos closely resembled those of *kdrl*$^{-/-}$ fish.

Scale bars: 50 μm in **D**, **G**, **R**, and **T**; 1 mm in **P**.

Figure 2

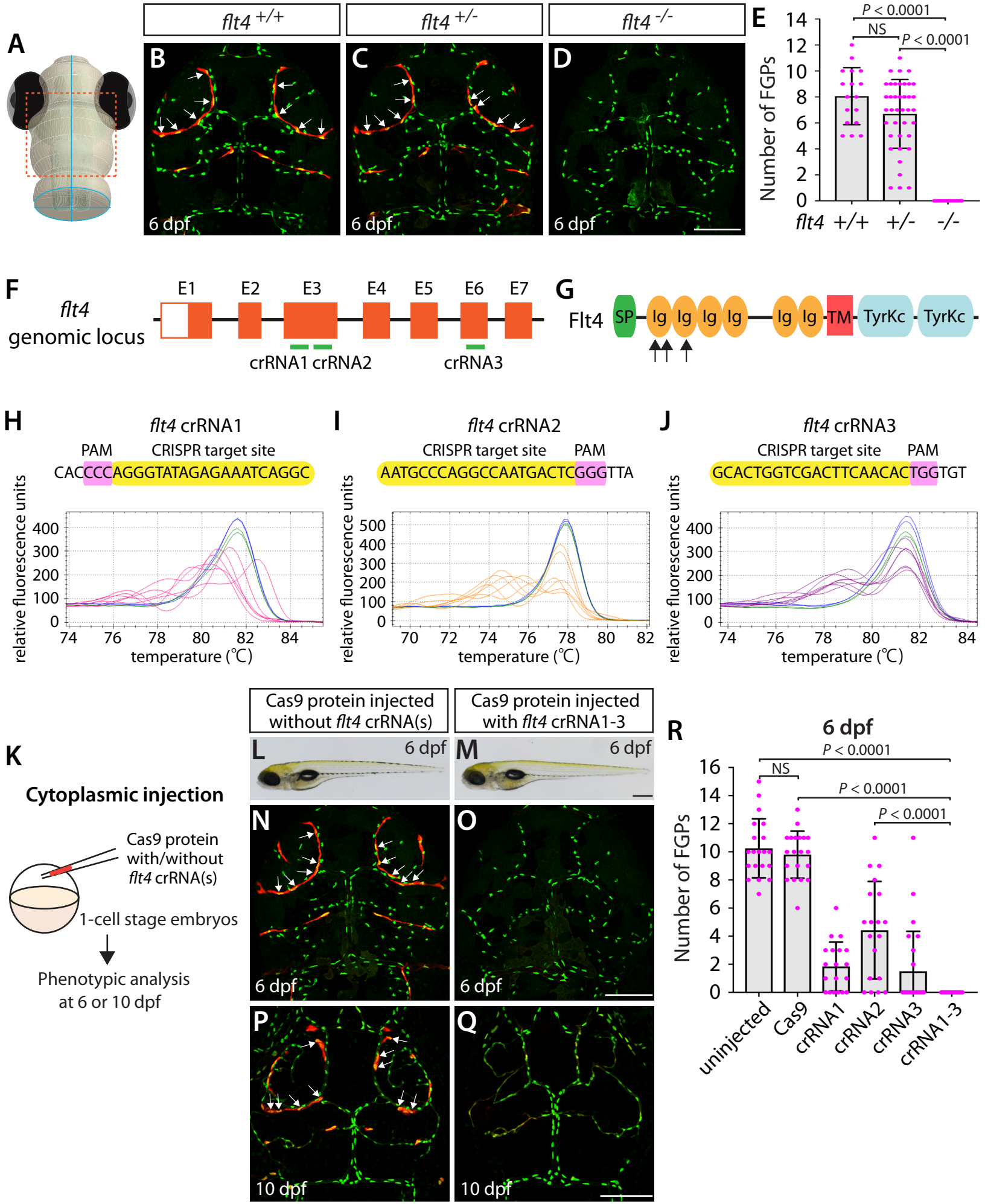
A
flt4 +/+
flt4 +/-
flt4 -/-
B
C
D
6 dpf
E
P < 0.0001
NS
P < 0.0001
Number of FGPs
flt4 +/+ +/- -/-
F
flt4 genomic locus
E1 E2 E3 E4 E5 E6 E7
crRNA1 crRNA2
crRNA3
G
Flt4
SP Ig Ig Ig Ig Ig Ig TM TyrKc TyrKc
H
flt4 crRNA1
PAM
CRISPR target site
CACCCCAGGGTATAGAGAAATCAGGC
relative fluorescence units
temperature (℃)
I
flt4 crRNA2
CRISPR target site
PAM
AATGCCCAGGCCAATGACTCGGGTTA
J
flt4 crRNA3
CRISPR target site
PAM
GCACTGGTCGACTTCAACACTGGTGT
K
Cytoplasmic injection
Cas9 protein with/without flt4 crRNA(s)
1-cell stage embryos
Phenotypic analysis at 6 or 10 dpf
Cas9 protein injected without flt4 crRNA(s)
Cas9 protein injected with flt4 crRNA1-3
L
M
N
O
P
Q
10 dpf
R
6 dpf
uninjected
Cas9
crRNA1
crRNA2
crRNA3
crRNA1-3

Figure 2. Triple *flt4* dgRNPs-injected larvae phenocopied the complete absence of brain meningeal perivascular FGPs observed in *flt4*$^{-/-}$ fish.

(**A**) Schematic representation of the dorsal view of the zebrafish larval head. The boxed area indicates the approximate region where the confocal images of panels (**B**–**D**) were captured.

(**B**–**D**) Dorsal head views of 6 dpf *flt4*$^{+/+}$, *flt4*$^{+/-}$, and *flt4*$^{-/-}$ larvae carrying *Tg(fli1:nEGFP)* and *Tg(lyve1:DsRed)* transgenes. While *flt4*$^{+/+}$ and *flt4*$^{+/-}$ larvae formed *Tg(fli1:*nEGFP*);Tg(lyve1:*DsRed*)*-double positive FGPs in the dorsal meningeal surfaces over the optic tectum (arrows, **B** and **C**), *flt4*$^{-/-}$ larvae completely lacked FGPs (**D**).

(**E**) Quantification of *Tg(fli1:*nEGFP*);Tg(lyve1:*DsRed*)*-double positive FGPs in the dorsal meningeal surfaces over the optic tectum for each genotype at 6 dpf (n=17 for *flt4*$^{+/+}$, n=39 for *flt4*$^{+/-}$, and n=21 for *flt4*$^{-/-}$ fish). NS: not significant.

(**F**) Three synthetic crRNAs were designed to target sequences within exon 3 (E3), and E6 on the *flt4* genomic locus.

(**G**) Predicted domain structure of zebrafish Flt4. Flt4 consists of a signal peptide (SP), six immunoglobulin-like domains (Ig), a transmembrane domain (TM), and two tyrosine kinase domains (TyrKc). Arrows indicate the approximate positions of the protein sequences corresponding to the target sequences of the three designed crRNAs.

(**H**–**J**) High-resolution melt analysis used to validate the efficacy of the three designed crRNAs. The melting curves of 6 independent embryos injected with the dgRNP complex consisting of *flt4* crRNA1 (**H**, **pink**), crRNA2 (**I**, **orange**), or crRNA3 (**J**, **purple**) are presented. The melting curves of 2 independent, uninjected (**H**–**J**, **blue**) and Cas9 protein-injected (**H**–**J**, **green**) sibling embryos are also presented for comparison for each crRNA. Injection of each dgRNP cocktail disrupted the corresponding target genomic sequences.

(**K**) Experimental workflow of the microinjection experiments for panels (**L**–**P**). Injection cocktails containing Cas9 protein with and without the individual or the three *flt4* crRNA:tracrRNA duplex complexes were injected into the cytoplasm of one-cell stage *Tg(fli1:nEGFP);Tg(lyve1:DsRed)* embryos. Injected progeny were analyzed at 6 and 10 dpf for FGP formation in the dorsal meningeal surfaces over the optic tectum.

(**L** and **M**) Brightfield images of the 6 dpf larvae injected with Cas9 protein with (**M**) or without (**L**) the three *flt4* crRNA:tracrRNA duplex complexes (crRNA1-3).

(**N**–**Q**) Dorsal head views of the 6 (**N**, **O**) and 10 (**P**, **Q**) dpf *Tg(fli1:nEGFP);Tg(lyve1:DsRed)* larvae injected with Cas9 protein with (**O**, **Q**) or without (**N**, **P**) the three *flt4* crRNA1-3. While Cas9 protein alone-injected larvae exhibited a bilateral loop of FGPs in the dorsal meningeal surfaces over the optic tectum at 6 and 10 dpf (arrows, **N** and **P**), those injected with the three *flt4* dgRNPs displayed a complete absence of the FGPs at both stages (**O** and **Q**).

(**R**) Quantification of *Tg(fli1:*nEGFP*);Tg(lyve1:*DsRed*)*-double positive FGPs in the dorsal meningeal surfaces over the optic tectum at 6 dpf (the number of the animals examined: n=20 for uninjected and Cas9 controls, n=19 for crRNA1 and crRNA2, n=24 for crRNA3, and n=26 for crRNA1-3). Larvae injected with all three *flt4* dgRNPs failed to form FGPs. Fish injected with the individual *flt4* dgRNPs displayed varying degrees of milder disruption to FGP formation. NS: not significant.

Scale bars: 50 μm in **D**, **O**, and **Q**; 1 mm in **M**.

Figure 3

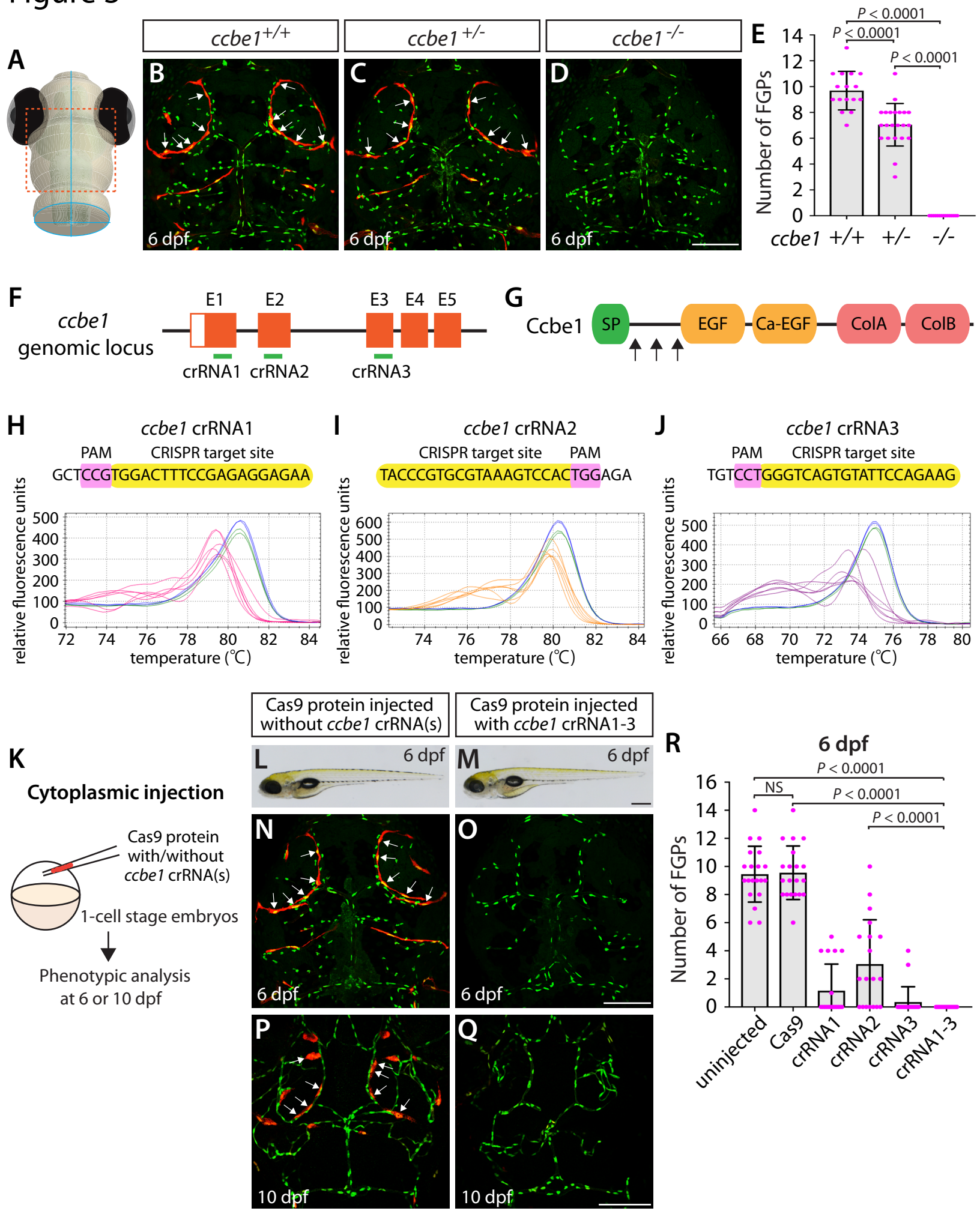
A
ccbe1+/+
ccbe1+/-
ccbe1-/-
B
C
D
6 dpf
E
P < 0.0001
P < 0.0001
P < 0.0001
Number of FGPs
ccbe1 +/+ +/- -/-
F
ccbe1 genomic locus
E1 E2 E3 E4 E5
crRNA1 crRNA2 crRNA3
G
Ccbe1
SP EGF Ca-EGF ColA ColB
H
ccbe1 crRNA1
PAM CRISPR target site
GCTCCGTGGACTTTCCGAGAGGAGAA
relative fluorescence units
temperature (℃)
I
ccbe1 crRNA2
CRISPR target site PAM
TACCCGTGCGTAAAGTCCACTGGAGA
J
ccbe1 crRNA3
PAM CRISPR target site
TGTCCTGGGTCAGTGTATTCCAGAAG
K
Cytoplasmic injection
Cas9 protein with/without ccbe1 crRNA(s)
1-cell stage embryos
Phenotypic analysis at 6 or 10 dpf
Cas9 protein injected without ccbe1 crRNA(s)
Cas9 protein injected with ccbe1 crRNA1-3
L
M
N
O
P
Q
10 dpf
R
6 dpf
P < 0.0001
NS
P < 0.0001
P < 0.0001
uninjected
Cas9
crRNA1
crRNA2
crRNA3
crRNA1-3

Figure 3. Triple *ccbe1* dgRNPs-injected larvae phenocopied the complete loss of brain meningeal perivascular FGPs observed in *ccbe1*$^{-/-}$ fish.

(**A**) Schematic representation of the dorsal view of the zebrafish larval head. The boxed area indicates the approximate region where the confocal images of panels (**B**–**D**) were captured.

(**B**–**D**) Dorsal head views of 6 dpf *ccbe1*$^{+/+}$, *ccbe1*$^{+/-}$, and *ccbe1*$^{-/-}$ larvae carrying *Tg(fli1:nEGFP)* and *Tg(lyve1:DsRed)* transgenes. While *ccbe1*$^{+/+}$ and *ccbe1*$^{+/-}$ larvae formed *Tg(fli1:*nEGFP*);Tg(lyve1:*DsRed*)*-double positive FGPs in the dorsal surfaces of the brain meninges over the optic tectum (arrows, **B** and **C**), *ccbe1*$^{-/-}$ larvae completely lacked FGPs (**D**).

(**E**) Quantification of *Tg(fli1:*nEGFP*);Tg(lyve1:*DsRed*)*-double positive FGPs in the dorsal meningeal surfaces over the optic tectum for each genotype at 6 dpf (n=16 for *ccbe1*$^{+/+}$, n=22 for *ccbe1*$^{+/-}$, and n=15 for *ccbe1*$^{-/-}$ fish).

(**F**) Three synthetic crRNAs were designed to target sequences within exon 1 (E1), E2 and E3 on the *ccbe1* genomic locus.

(**G**) Predicted domain structure of zebrafish Ccbe1. Ccbe1 consists of a signal peptide (SP), an EGF domain (EGF), a calcium-binding EGF domain (Ca-EGF), and two collagen repeat domains (ColA and ColB). Arrows indicate the approximate positions of the protein sequences corresponding to the target sequences of the three designed crRNAs.

(**H**–**J**) High-resolution melt analysis used to validate the efficacy of the three designed crRNAs. The melting curves of 6 independent embryos injected with the dgRNP complex consisting of *ccbe1* crRNA1 (**H**, **pink**), crRNA2 (**I**, **orange**), or crRNA3 (**J**, **purple**) are presented. The melting curves of 2 independent, uninjected (**H**–**J**, **blue**) and Cas9 protein-injected (**H**–**J**, **green**) sibling embryos are also presented for comparison for each crRNA. Injection of each dgRNP cocktail disrupted the corresponding target genomic sequences.

(**K**) Experimental workflow of the microinjection experiments for panels (**L**–**P**). Injection cocktails containing Cas9 protein with and without the individual or the three *ccbe1* crRNA:tracrRNA duplex complexes were injected into the cytoplasm of one-cell stage *Tg(fli1:nEGFP);Tg(lyve1:DsRed)* embryos. Injected progeny were analyzed at 6 and 10 dpf for FGP formation in the dorsal meningeal surfaces over the optic tectum.

(**L** and **M**) Brightfield images of the 6 dpf larvae injected with Cas9 protein with (**M**) or without (**L**) the three *ccbe1* crRNA:tracrRNA duplex complexes (crRNA1-3).

(**N**–**Q**) Dorsal head views of the 6 (**N**, **O**) and 10 (**P**, **Q**) dpf *Tg(fli1:nEGFP);Tg(lyve1:DsRed)* larvae injected with Cas9 protein with (**O**, **Q**) or without (**N**, **P**) the three *ccbe1* crRNA1-3. Cas9 protein alone-injected larvae exhibited a bilateral loop of FGPs in the dorsal meningeal surfaces over the optic tectum at 6 and 10 dpf (arrows, **N** and **P**). However, fish injected with the three *ccbe1* dgRNPs completely lacked the FGPs at both stages (**O** and **Q**).

(**R**) Quantification of *Tg(fli1:*nEGFP*);Tg(lyve1:*DsRed*)*-double positive FGPs in the dorsal meningeal surfaces over the optic tectum at 6 dpf (the number of the animals examined: n=20 for uninjected and Cas9 controls, n=19 for crRNA1 and crRNA2, n=20 for crRNA3, and n=22 for crRNA1-3). All larvae injected with the three *ccbe1* dgRNPs exhibited a complete absence of FGPs over the optic tectum. Fish injected with the individual *ccbe1* dgRNPs displayed varying degrees of milder disruption to FGP formation. NS: not significant.

Scale bars: 50 μm in **D**, **O**, and **Q**; 1 mm in **M**.

Figure 4

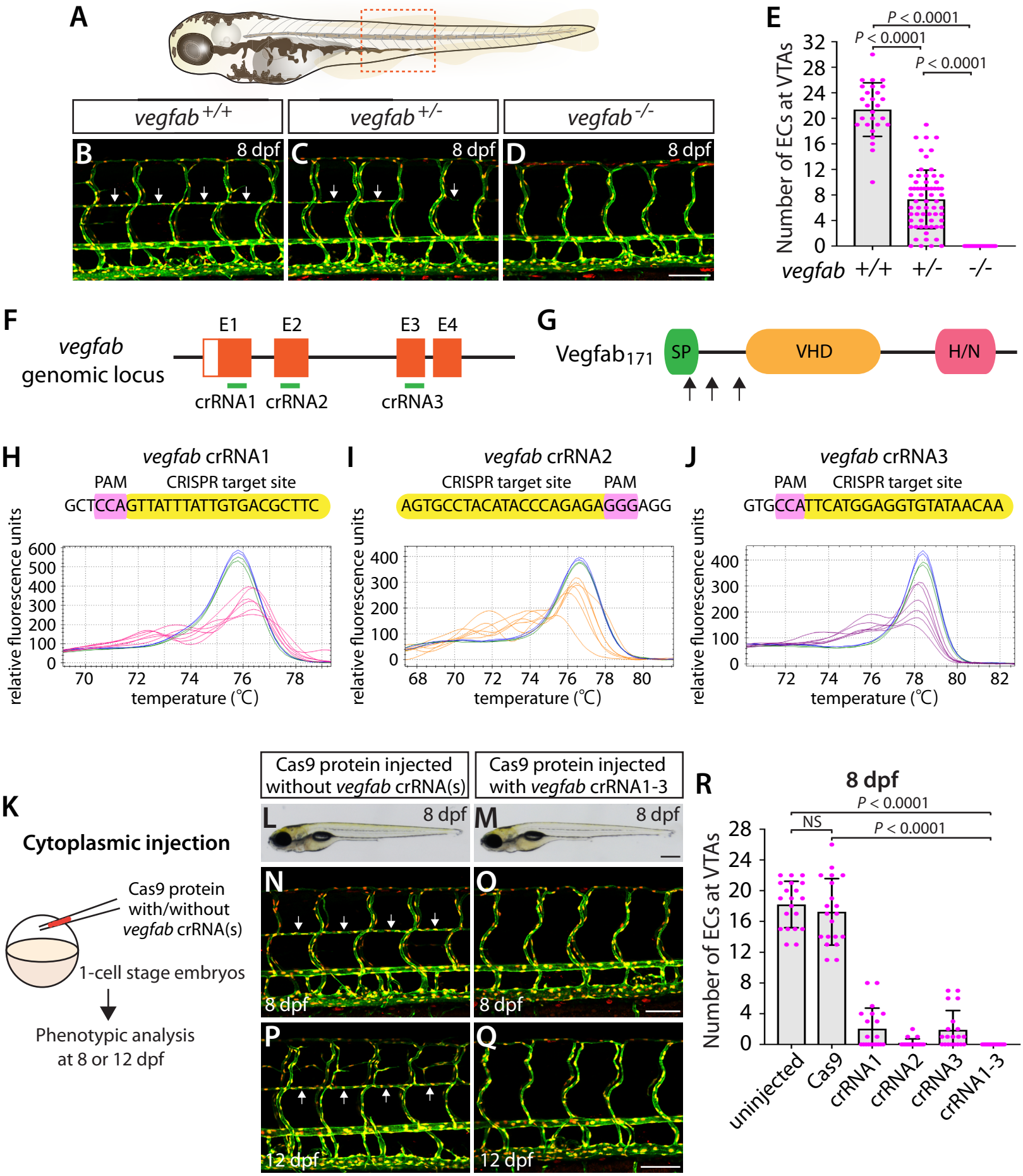
A
vegfab +/+
vegfab +/-
vegfab -/-
B
8 dpf
C
8 dpf
D
8 dpf
E
P < 0.0001
P < 0.0001
P < 0.0001
Number of ECs at VTAs
vegfab +/+ +/- -/-
F
vegfab genomic locus
E1 E2 E3 E4
crRNA1 crRNA2 crRNA3
G
Vegfab171
SP
VHD
H/N
H
vegfab crRNA1
PAM
CRISPR target site
GCTCCAGTTATTTATTGTGACGCTTC
relative fluorescence units
temperature (℃)
I
vegfab crRNA2
CRISPR target site
PAM
AGTGCCTACATACCCAGAGAGGGAGG
relative fluorescence units
temperature (℃)
J
vegfab crRNA3
PAM
CRISPR target site
GTGCCATTCATGGAGGTGTATAACAA
relative fluorescence units
temperature (℃)
K
Cytoplasmic injection
Cas9 protein with/without vegfab crRNA(s)
1-cell stage embryos
Phenotypic analysis at 8 or 12 dpf
Cas9 protein injected without vegfab crRNA(s)
Cas9 protein injected with vegfab crRNA1-3
L
8 dpf
M
8 dpf
N
8 dpf
O
8 dpf
P
12 dpf
Q
12 dpf
R
8 dpf
P < 0.0001
NS
P < 0.0001
Number of ECs at VTAs
uninjected
Cas9
crRNA1
crRNA2
crRNA3
crRNA1-3

Figure 4. Triple *vegfab* dgRNPs-injected larvae phenocopied the complete absence of VTAs observed in *vegfab*$^{-/-}$ fish.

(**A**) Schematic representation of the lateral view of an 8 dpf zebrafish larva. The boxed area indicates the approximate trunk region where all VTA analyses and quantifications were performed.

(**B**–**D**) Lateral trunk views of 8 dpf *vegfab*$^{+/+}$, *vegfab*$^{+/-}$, and *vegfab*$^{-/-}$ larvae carrying *Tg(kdrl:EGFP)* and *Tg(kdrl:NLS-mCherry)* transgenes. While *vegfab*$^{+/+}$ larvae formed most of VTAs that extended bilaterally along the ventrolateral sides of the spinal cord (**B**, arrows), *vegfab*$^{-/-}$ larvae completely lacked VTAs (**D**). Most *vegfab*$^{+/-}$ larvae exhibited partially forming VTAs at this stage (**C**, arrows).

(**E**) Quantification of *Tg(kdrl:*EGFP*);Tg(kdrl:*NLS-mCherry*)*-double positive ECs at the VTAs within a 5 somite region per animal at 8 dpf (n=27 for *vegfab*$^{+/+}$, n=64 for *vegfab*$^{+/-}$, and n=35 for *vegfab*$^{-/-}$ fish).

(**F**) Three synthetic crRNAs were designed to target sequences within exon 1 (E1), E2, and E3 on the *vegfab* genomic locus.

(**G**) Predicted domain structure of zebrafish Vegfab$_{171}$ isoform. Vegfab$_{171}$ consists of a signal peptide (SP), a VEGF homology domain (VHD), and a heparin and neuropilin1 binding domain (H/N). Arrows indicate the approximate positions of the protein sequences corresponding to the target sequences of the three designed crRNAs.

(**H**–**J**) High-resolution melt analysis used to validate the efficacy of the three designed crRNAs. The melting curves of 6 independent embryos injected with the dgRNP complex consisting of *vegfab* crRNA1 (**H**, **pink**), crRNA2 (**I**, **orange**), or crRNA3 (**J**, **purple**) are presented. The melting curves of 2 independent, uninjected (**H**–**J**, **blue**) and Cas9 protein-injected (**H**–**J**, **green**) sibling embryos are also presented for comparison for each crRNA. Injection of each dgRNP cocktail disrupted the corresponding target genomic sequences.

(**K**) Experimental workflow of the microinjection experiments for panels (**L**–**P**). Injection cocktails containing Cas9 protein with and without the individual or the three *vegfab* crRNA:tracrRNA duplex complexes were injected into the cytoplasm of one-cell stage *Tg(kdrl:EGFP);Tg(kdrl:NLS-mCherry)* embryos. Injected progeny were analyzed for VTA formation at 8 and 12 dpf.

(**L** and **M**) Brightfield images of the 8 dpf larvae injected with Cas9 protein with (**M**) or without (**L**) the three *vegfab* crRNA:tracrRNA duplex complexes (crRNA1-3).

(**N**–**Q**) Lateral trunk views of the 8 (**N**, **O**) and 12 (**P**, **Q**) dpf *Tg(kdrl:EGFP);Tg(kdrl:NLS-mCherry)* larvae injected with Cas9 protein with (**O**, **Q**) or without (**N**, **P**) the three *vegfab* crRNA1-3. While Cas9 protein alone-injected larvae formed most of the VTAs at 8 and 12 dpf (arrows, **N** and **P**), those injected with the three *vegfab* dgRNPs displayed a complete absence of VTAs at both stages (**O** and **Q**).

(**R**) Quantification of the number of ECs comprising the VTAs within a 5 somite region per animal at 8 dpf (the number of the animals examined: n=20 for uninjected and Cas9 controls, n=20 for crRNA1, crRNA2, and crRNA3, and n=27 for crRNA1-3). All larvae injected with the three *vegfab* dgRNPs failed to form VTAs. Fish injected with the individual *vegfab* dgRNPs displayed varying degrees of milder disruption to VTA formation. NS: not significant.

Scale bars: 50 μm in **D**, **O**, and **Q**; 1 mm in **M**.

Figure 5

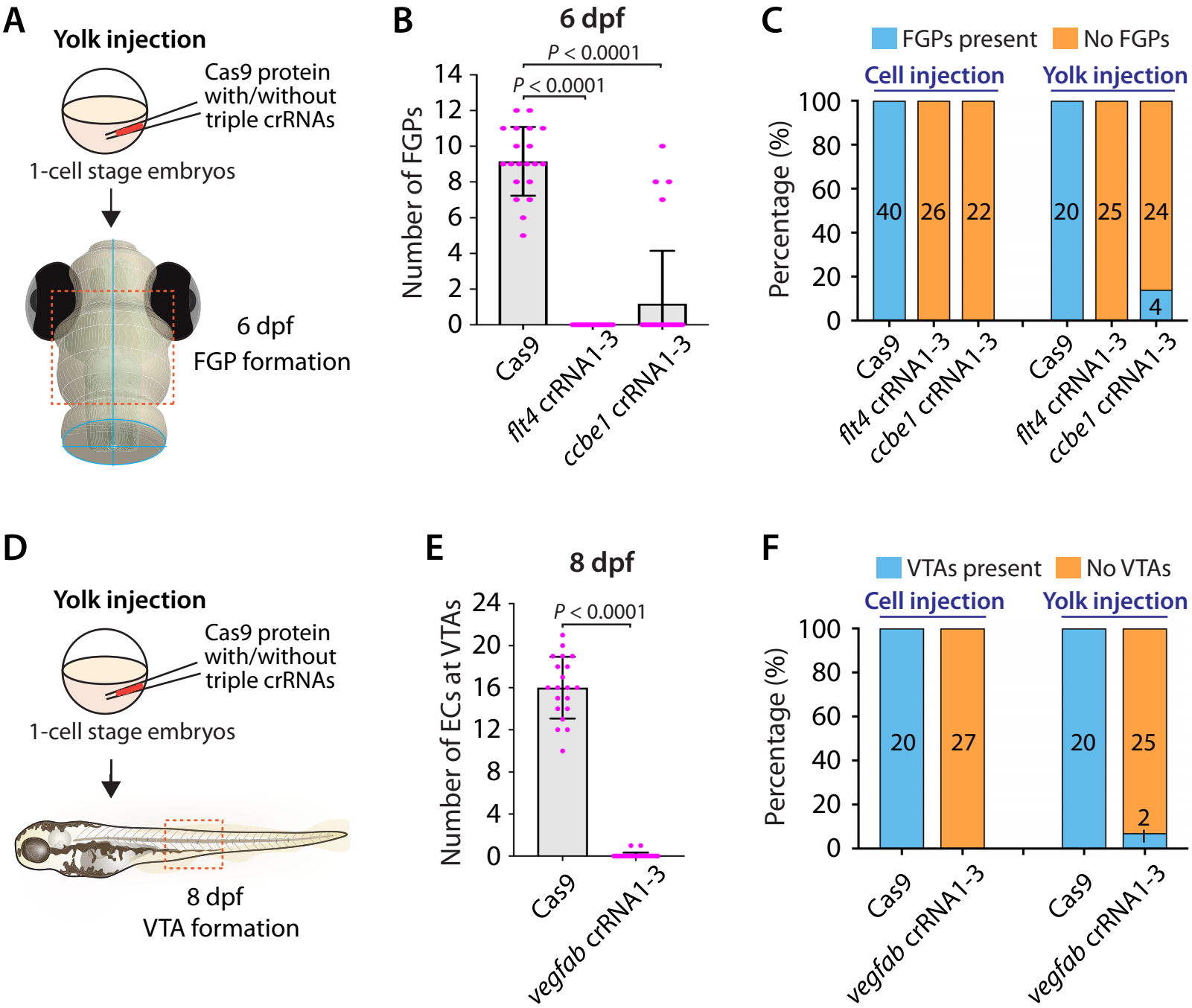

G

Injection site	Cytoplasm				Yolk
Gene \ crRNA	crRNA1	crRNA2	crRNA3	crRNA1-3	crRNA1-3
flt4	32% (n=19)	21% (n=19)	71% (n=24)	100% (n=26)	100% (n=25)
ccbe1	68% (n=19)	37% (n=19)	90% (n=20)	100% (n=22)	86% (n=28)
vegfab	50% (n=20)	85% (n=20)	40% (n=20)	100% (n=27)	93% (n=27)

Figure 5. Yolk injections of three dgRNPs per gene allowed efficient generation of biallelic F0 knockouts.

(**A**) Experimental workflow of the yolk microinjection experiments for panel (**B**). Injection cocktails containing Cas9 protein with and without the three *flt4* or *ccbe1* crRNA:tracrRNA duplex complexes were injected into the yolk of one-cell stage *Tg(fli1:nEGFP);Tg(lyve1:DsRed)* embryos. Injected progeny were analyzed at 6 dpf for FGP formation in the dorsal meningeal surfaces over the optic tectum.

(**B**) Quantification of *Tg(fli1:*nEGFP*);Tg(lyve1:*DsRed*)*-double positive FGPs in the dorsal meningeal surfaces over the optic tectum at 6 dpf after yolk injection of Cas9 protein with and without the three *flt4* or *ccbe1* crRNA:tracrRNA duplex complexes (the number of the animals examined: n=20 for Cas9 controls, n=26 for *flt4* crRNA1-3, and n=28 for *ccbe1* crRNA1-3). All *flt4* dgRNPs-injected larvae failed to form FGPs in the dorsal meningeal surfaces over the optic tectum. Approximately 86% of *ccbe1* dgRNPs-injected larvae completely lacked FGPs, but the remaining fish formed FGPs in a manner comparable to Cas9-injected controls.

(**C**) Percentage of 6 dpf larvae of indicated treatment with and without FGPs in the dorsal meningeal surfaces over the optic tectum (the number of the animals examined for each group is listed in the panel). Cytoplasmic and yolk injection results are presented for *flt4* and *ccbe1* dgRNPs.

(**D**) Experimental workflow of the yolk microinjection experiments for panel (**E**). Injection cocktails containing Cas9 protein with and without the three *vegfab* crRNA:tracrRNA duplex complexes were injected into the yolk of one-cell stage *Tg(kdrl:EGFP);Tg(kdrl:NLS-mCherry)* embryos. Injected progeny were analyzed for VTA formation at 8 dpf.

(**E**) Quantification of *Tg(kdrl:*EGFP*);Tg(kdrl:*NLS-mCherry*)*-double positive ECs at the VTAs within a 5 somite region per animal at 8 dpf after yolk injection of Cas9 protein with and without the three *vegfab* crRNA:tracrRNA duplex complexes (the number of the animals examined: n=20 for Cas9 controls and n=27 for *vegfab* crRNA1-3).

(**F**) Percentage of larvae of indicated treatment with and without VTAs within a 5 somite region per animal at 8 dpf (the number of the animals examined for each group is listed in the panel). Cytoplasmic and yolk injection results are presented for *vegfab* dgRNPs.

(**G**) A summary table listing the percentage of larvae of indicated treatment that displayed biallelic mutant vascular phenotypes. A complete absence of FGPs at 6 dpf (*flt4* and *ccbe1*), or of VTAs at 8 dpf (*vegfab*), were defined as biallelic mutant vascular phenotypes.

Figure 6

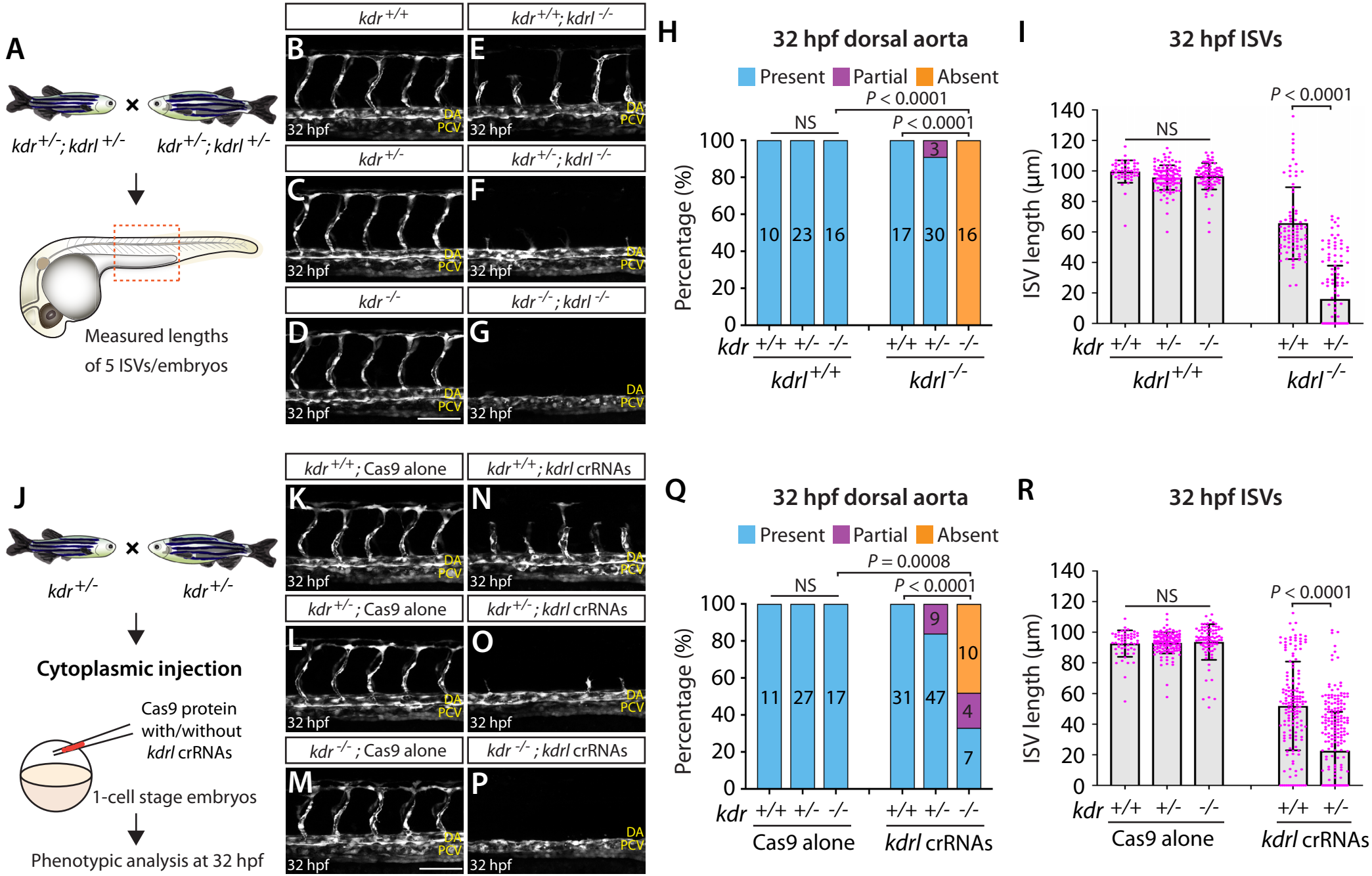
A
kdr+/-; kdrl+/-
kdr+/-; kdrl+/-
Measured lengths of 5 ISVs/embryos
kdr+/+
kdr+/+; kdrl-/-
kdr+/-
kdr+/-; kdrl-/-
kdr-/-
kdr-/-; kdrl-/-
B
C
D
E
F
G
32 hpf
DA
PCV
H
32 hpf dorsal aorta
Present
Partial
Absent
P < 0.0001
NS
P < 0.0001
Percentage (%)
10
23
16
17
30
16
3
kdr +/+ +/- -/-
+/+ +/- -/-
kdrl+/+
kdrl-/-
I
32 hpf ISVs
P < 0.0001
NS
ISV length (µm)
kdr +/+ +/- -/-
+/+ +/-
kdrl+/+
kdrl-/-
J
kdr+/-
kdr+/-
Cytoplasmic injection
Cas9 protein with/without kdrl crRNAs
1-cell stage embryos
Phenotypic analysis at 32 hpf
kdr+/+; Cas9 alone
kdr+/+; kdrl crRNAs
kdr+/-; Cas9 alone
kdr+/-; kdrl crRNAs
kdr-/-; Cas9 alone
kdr-/-; kdrl crRNAs
K
L
M
N
O
P
Q
32 hpf dorsal aorta
Present
Partial
Absent
P = 0.0008
NS
P < 0.0001
Percentage (%)
11
27
17
31
47
9
10
4
7
kdr +/+ +/- -/-
+/+ +/- -/-
Cas9 alone
kdrl crRNAs
R
32 hpf ISVs
NS
P < 0.0001
ISV length (µm)
kdr +/+ +/- -/-
+/+ +/-
Cas9 alone
kdrl crRNAs

Figure 6. Genetic interaction analysis of the two Vegfr2 zebrafish paralogs, Kdr and Kdrl, in the formation of the dorsal aorta and aISVs.

(**A**) Experimental workflow of the phenotypic analysis presented in panels (**B**–**I**). Adult *kdr*$^{+/-}$;*kdrl*$^{+/-}$ fish were incrossed, and progeny generated from the crosses were imaged to analyze the formation of the dorsal aorta and aISVs at 32 hpf.

(**B**–**G**) Lateral views of *kdr*$^{+/+}$ (**B**), *kdr*$^{+/-}$ (**C**), *kdr*$^{-/-}$ (**D**), *kdr*$^{+/+}$;*kdrl*$^{-/-}$ (**E**), *kdr*$^{+/-}$;*kdrl*$^{-/-}$ (**F**), and *kdr*$^{-/-}$;*kdrl*$^{-/-}$ (**G**) trunk vasculature visualized by *Tg(kdrl:*EGFP*)* expression at 32 hpf. No obvious trunk vascular defects were observed in *kdr*$^{+/+}$, *kdr*$^{+/-}$, and *kdr*$^{-/-}$ embryos (**B**–**D**). *kdr*$^{+/+}$;*kdrl*$^{-/-}$ embryos exhibited stalled aISV growth (**E**), and this aISV growth defect was exacerbated in *kdr*$^{+/-}$;*kdrl*$^{-/-}$ embryos (**F**). In all *kdr*$^{-/-}$;*kdrl*$^{-/-}$ embryos examined at 32 hpf, the dorsal aorta failed to form (**G**). DA: dorsal aorta; PCV: posterior cardinal vein.

(**H**) Percentage of 32 hpf embryos of indicated genotype in the presence, partial presence, and absence of the dorsal aorta (the number of the animals examined per genotype is listed in the panel).

(**I**) Quantification of aISV lengths of 32 hpf embryos of the indicated genotypes (n=10 for *kdr*$^{+/+}$, n=23 for *kdr*$^{+/-}$, n=16 for *kdr*$^{-/-}$, n=17 for *kdr*$^{+/+}$;*kdrl*$^{-/-}$, and n=29 for *kdr*$^{+/-}$;*kdrl*$^{-/-}$; 5 aISV lengths per embryo measured). *kdr*$^{+/-}$;*kdrl*$^{-/-}$ embryos displayed significantly shorter average aISV lengths than those of *kdr*$^{+/+}$;*kdrl*$^{-/-}$ fish.

(**J**) Experimental workflow of the microinjection experiments for panels (**K**–**R**). Injection cocktails containing Cas9 protein with and without the three *kdrl* crRNA:tracrRNA duplex complexes were injected into the cytoplasm of one-cell stage embryos generated from incrosses of *kdr*$^{+/-}$ fish carrying the *Tg(kdrl:EGFP)* transgene. Injected progeny were imaged to analyze the formation of the dorsal aorta and aISVs at 32 hpf.

(**K**–**P**) Lateral trunk views of the 32 hpf *kdr*$^{+/+}$ (**K**, **N**), *kdr*$^{+/-}$ (**L**, **O**), and *kdr*$^{-/-}$ (**M**, **P**) embryos injected with Cas9 protein with (**N**–**P**) or without (**K**–**M**) the three *kdrl* crRNA:tracrRNA duplex complexes (*kdrl* crRNAs). Trunk vasculature was visualized by *Tg(kdrl:*EGFP*)* expression. No obvious trunk vascular defects were observed in *kdr*$^{+/+}$, *kdr*$^{+/-}$, and *kdr*$^{-/-}$ embryos injected with Cas9 protein alone (**K**–**M**). In contrast, *kdr*$^{+/+}$ embryos injected with the three *kdrl* dgRNP cocktail displayed the stalled aISV phenotype (**N**). More severe aISV growth defects were observed in the *kdr*$^{+/-}$ embryos injected with the three *kdrl* dgRNPs (**O**). A nearly half of the three *kdrl* dgRNPs-injected *kdr*$^{-/-}$ embryos exhibited a complete absence of the dorsal aorta (**P**).

(**Q**) Percentage of 32 hpf embryos of the indicated genotype and treatment in the presence, partial presence, and absence of the dorsal aorta (the number of the animals examined per group is listed in the panel).

(**R**) Quantification of aISV lengths of 32 hpf embryos of the indicated genotype and treatment (n=11 for Cas9-injected *kdr*$^{+/+}$, n=27 for Cas9-injected *kdr*$^{+/-}$, n=17 for Cas9-injected *kdr*$^{-/-}$, n=31 for *kdrl* crRNAs-injected *kdr*$^{+/+}$, and n=54 for *kdrl* crRNAs-injected *kdr*$^{+/-}$; 5 aISV lengths per embryo measured). *kdr*$^{+/-}$ embryos injected with the three *kdrl* dgRNP cocktail exhibited significantly shorter average aISV lengths than those of the same dgRNPs-injected *kdr*$^{+/+}$ fish.

Scale bars: 50 μm. NS: not significant.

Figure S1

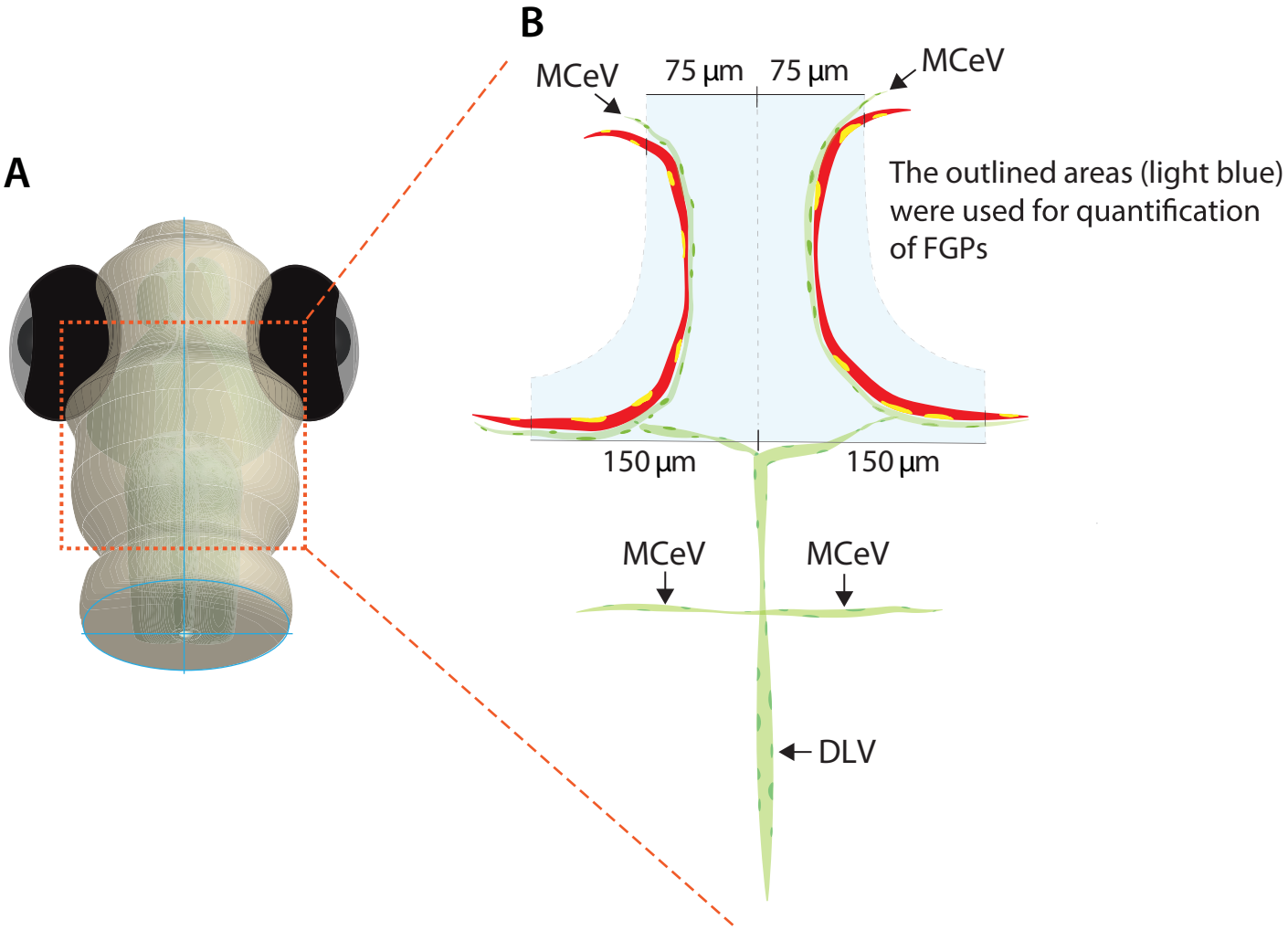

Figure S1. Quantification of FGPs over the optic tectum.

(**A**) Schematic representation of the dorsal view of the zebrafish larval head. The boxed area indicates the approximate location where the confocal images of bilateral *Tg(lyve1:*DsRed*)*$^{+}$ loops over the optic tectum were captured.

(**B**) Schematic diagram of the vasculature (green) and bilateral *Tg(lyve1:*DsRed*)*$^{+}$ loops (red) over the optic tectum. The areas in which FGPs were quantified are highlighted in light blue. The number of *Tg(fli1:*nEGFP*);Tg(lyve1:*DsRed*)*-double positive FGPs (yellow) within the highlighted area were recorded.

Figure S2

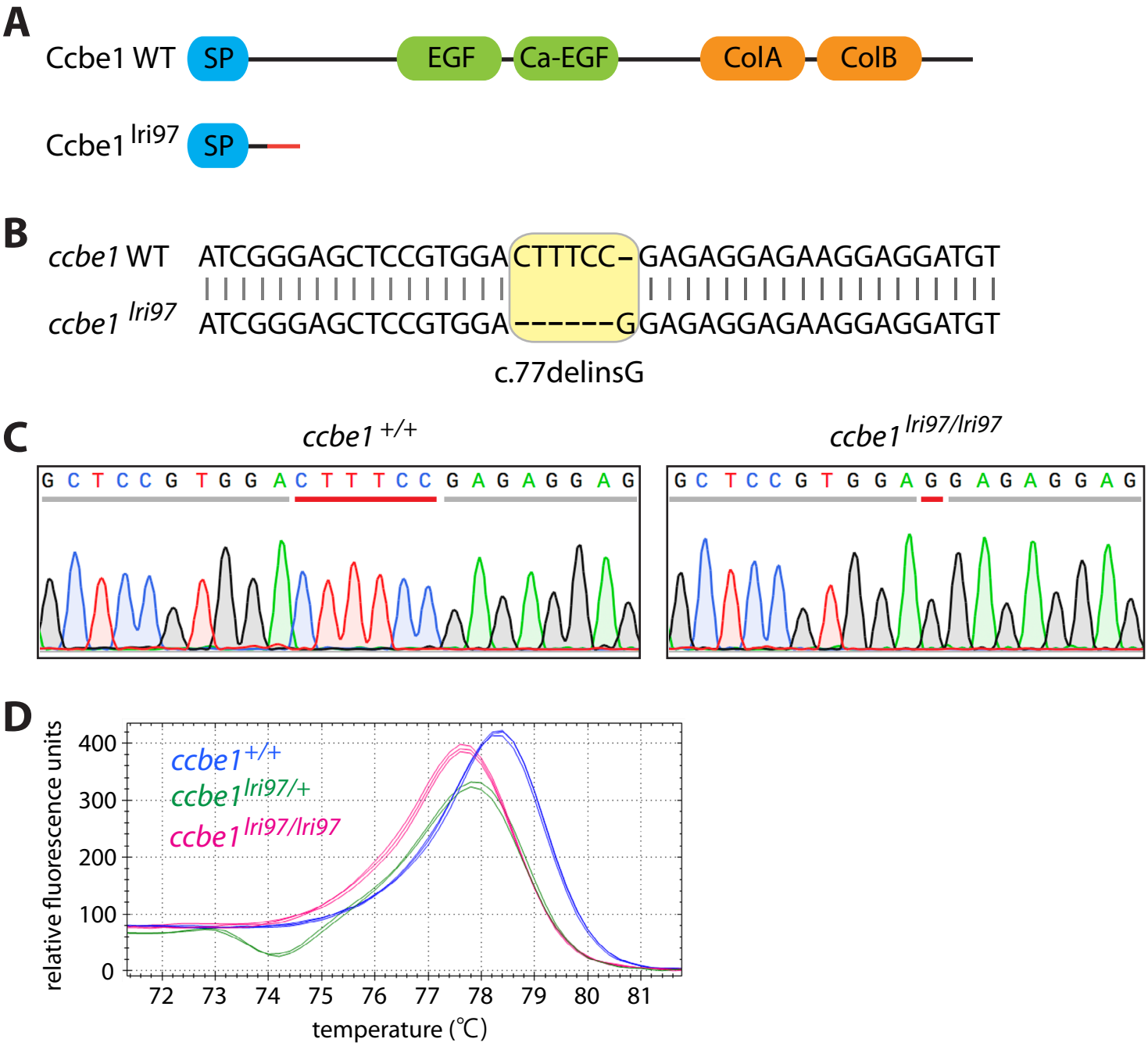

Figure S2. Generation and validation of zebrafish *ccbe1*^{lri97} mutant allele.

(**A**) Predicted protein structure of zebrafish WT Ccbe1 and Ccbe1^{lri97}. WT Ccbe1 consists of a signal peptide (SP), an EGF domain (EGF), a calcium-binding EGF domain (Ca-EGF), and two collagen repeat domains (ColA and ColB). Ccbe1^{lri97} is expected to lack all functional domains except a SP. The red solid line of Ccbe1^{lri97} represents missense sequences downstream of the mutation before the stop codon.

(**B** and **C**) Sequence alignment of part of exon 1 from the *ccbe1*$^{+/+}$ and *ccbe1*$^{lri97/lri97}$ allele shows CRISPR-induced indels (**B**). A six-nucleotide deletion (CTTTCC) and a one-nucleotide insertion (G) in the *ccbe1*$^{lri97/lri97}$ allele were confirmed by the sequence chromatograms of the PCR products generated using *ccbe1*$^{+/+}$ and *ccbe1*$^{lri97/lri97}$ fish genomic DNA as templates (**C**). Red lines in the sequence chromatograms indicate the CRISPR-induced nucleotide changes between *ccbe1*$^{+/+}$ and *ccbe1*$^{lri97/lri97}$ fish.

(**D**) High-resolution melt analysis was used to determine the *ccbe1*^{lri97} genotypes. Melting curves for 2-3 independent fish of each genotype are shown in different colors as indicated in the panel.